
This is an electronic reprint of the original article.

This reprint may differ from the original in pagination and typographic detail.

Singh, Anamika; Asikainen, Sanja; Teotia, Arun K.; Shiekh, Parvaiz A.; Huotilainen, Eero; Qayoom, Irfan; Partanen, Jouni; Seppälä, Jukka; Kumar, Ashok

Biomimetic Photocurable Three-Dimensional Printed Nerve Guidance Channels with Aligned Cryomatrix Lumen for Peripheral Nerve Regeneration

Published in:
ACS Applied Materials and Interfaces

DOI:
[10.1021/acsami.8b11677](https://doi.org/10.1021/acsami.8b11677)

Published: 19/12/2018

Document Version
Peer-reviewed accepted author manuscript, also known as Final accepted manuscript or Post-print

Published under the following license:
Unspecified

Please cite the original version:
Singh, A., Asikainen, S., Teotia, A. K., Shiekh, P. A., Huotilainen, E., Qayoom, I., Partanen, J., Seppälä, J., & Kumar, A. (2018). Biomimetic Photocurable Three-Dimensional Printed Nerve Guidance Channels with Aligned Cryomatrix Lumen for Peripheral Nerve Regeneration. *ACS Applied Materials and Interfaces*, 10(50), 43327-43342. <https://doi.org/10.1021/acsami.8b11677>

**Biomimetic Photocurable 3D Printed Nerve Guidance Channels
with Aligned Cryomatrix Lumen for Peripheral Nerve Regeneration**Anamika Singh, Sanja Asikainen, Arun Kumar Teotia, Parvaiz Ahmad Shiekh, Eero
Huotilainen, Irfan Qayoom, Jouni Partanen, Jukka V. Seppälä, and Ashok KumarACS Appl. Mater. Interfaces, **Just Accepted Manuscript** • DOI: 10.1021/acsami.8b11677 • Publication Date (Web): 21 Nov 2018Downloaded from <http://pubs.acs.org> on November 22, 2018**Just Accepted**

“Just Accepted” manuscripts have been peer-reviewed and accepted for publication. They are posted online prior to technical editing, formatting for publication and author proofing. The American Chemical Society provides “Just Accepted” as a service to the research community to expedite the dissemination of scientific material as soon as possible after acceptance. “Just Accepted” manuscripts appear in full in PDF format accompanied by an HTML abstract. “Just Accepted” manuscripts have been fully peer reviewed, but should not be considered the official version of record. They are citable by the Digital Object Identifier (DOI®). “Just Accepted” is an optional service offered to authors. Therefore, the “Just Accepted” Web site may not include all articles that will be published in the journal. After a manuscript is technically edited and formatted, it will be removed from the “Just Accepted” Web site and published as an ASAP article. Note that technical editing may introduce minor changes to the manuscript text and/or graphics which could affect content, and all legal disclaimers and ethical guidelines that apply to the journal pertain. ACS cannot be held responsible for errors or consequences arising from the use of information contained in these “Just Accepted” manuscripts.



Biomimetic Photocurable 3D Printed Nerve Guidance Channels with Aligned Cryomatrix Lumen for Peripheral Nerve Regeneration

Anamika Singh[†], Sanja Asikainen[‡], Arun K. Teotia[†], Parvaiz A. Shiekh[†], Eero Huotilainen[#], Irfan Qayoom[†], Jouni Partanen[#], Jukka Seppälä[‡] and Ashok Kumar^{†,‡,*}

[†]Department of Biological Sciences and Bioengineering, Indian Institute of Technology Kanpur, Kanpur-208016, India

[‡]Centre for Environmental Science and Engineering & Centre for Nanosciences, Indian Institute of Technology Kanpur, Kanpur-208016, India

[‡]Department of Chemical and Metallurgical Engineering, School of Chemical Engineering, Aalto University, Finland

[#]Department of Mechanical Engineering, School of Engineering, Aalto University, Finland

*Address for correspondence:

Prof. Ashok Kumar

Department of Biological Sciences and Bioengineering

Indian Institute of Technology Kanpur

Kanpur-208016

Tel.: +91-512-2594051

Fax: +91-512-2594010

Email: ashokkum@iitk.ac.in

Keywords: 3D printing, guidance channel, aligned cryogel, nerve regeneration, stereolithography

Abstract

Repair and regeneration of the critically injured peripheral nerves is one of the most challenging reconstructive surgeries. Currently available and FDA approved nerve guidance channels (NGCs) are suitable for small gap injuries, and their biological performance is inferior to that of autografts. Development of biomimetic NGCs with clinically relevant geometrical and biological characteristics such as topographical, biochemical and haptotactic cues could offer better regeneration of the long gap complex nerve injuries. Here, in this study, we present the development and preclinical analysis of a 3D printed aligned cryomatrix filled NGCs along with nerve growth factor (NGF) (aCG+NGF) for peripheral nerve regeneration. We demonstrated the application of these aCG+NGF NGCs in the enhanced and successful regeneration of a critically injured rat sciatic nerve in comparison to random cryogel filled NGCs, multichannel, and clinically preferred hollow conduits as well as gold standard autografts. Our results indicated viz-a-viz similar effect of aCG+NGF NGCs to that of autografts, and not only enhanced the overall regenerated nerve physiology, but could also mimic the cellular aspects of regeneration. This study emphasizes the paradigm that these biomimetic 3D printed NGCs will lead to a better functional regenerative outcome under clinical settings.

1. Introduction

Injuries to the nervous system are challenging to repair and regenerate due to intrinsic non-dividing nature of neural cells. According to United States and Europe statistical data, approximately 200,000 peripheral nerve repair procedures are performed annually.¹ The peripheral nervous system has some ingrained spontaneous nerve regeneration capability, limited to damaged nerves in cases of axonotmesis.² In cases of neurotmesis, where a gap has developed, the end to end repair is performed for 5 mm long cut size injuries. However, for larger gaps where tension is generated due to end to end repair, autografts are still preferred as the gold standard.^{3,4} The various limitations associated with autografts like donor site morbidity, limited availability, mismatch in size and painful neuroma formation lead to development of alternative strategies.⁵ So, as an alternative to autografts, nerve guidance scaffolds have been developed using both biological and synthetic materials like collagen, polycaprolactone, silk, etc.⁶ Some of these developed scaffolds are FDA approved and commercially available for nerve injuries. However, they fail to regenerate and regain the complete functional recovery after nerve injury and their performance is inferior to that of autografts.⁴ The commercially available nerve guiding scaffolds are hollow tubular bridging devices, primarily providing protection to regenerating axons against compression, inhibiting scar tissue formation at the site of injury and providing longitudinal guidance to the regenerating nerves. However, their capability to regenerate the fully transected nerve gaps is below par to that of autografts and are unable to provide guidance to the re-growing axons, leading to their misguidance and polyinnervation.⁷

To enhance the nerve regeneration for such critical injuries, nerve guiding scaffolds consisting of an external conduit filled with sponges, fibers and hydrogels have been fabricated. Further incorporation of microstructure patterning in the lumen of these conduits for axonal

regeneration have also been fabricated. Various studies have demonstrated the efficiency of these matrix filled conduits in regenerating nerves over the hollow conduits.^{8–12}

On the fabrication aspect, the guiding conduits have been developed using different conventional techniques such as electrospinning, porogen-leaching, freeze-drying, and solvent or thermally-induced phase separation.⁶ However, the formation of such unique micro structures needs a scalable fabrication technique having advantages over the traditional extrusion processes. Moreover, the nerve injuries may differ on the type of injury and dimensions of the injured nerve, indicating requirement for a personalized medical approach. With the recent advancements in fabrication technology, 3D printing technique led to the development of functionalized nerve regeneration scaffolds, mimicking anatomical nerve architecture with high resolution and scalability for nerve regeneration.^{13,14} 3D printing using stereolithography based on photopolymerisation is an emerging approach acclaimed in the last few decades for developing 3D objects.¹⁵ Nerve conduits with defined microstructures developed using stereolithography have shown peripheral nerve regeneration in in-vivo nerve injury model.^{16,17}

After a nerve injury, it is important for the proliferating Schwann cells (SCs) to arrange themselves into aligned structures known as Bands of Büngner to provide guidance cues to these re-growing axons from the injured neurons. Collagen-based aligned microstructured nerve guide Perimaix has shown enhanced nerve regeneration similar to autologous nerve transplantation.¹⁸ For that reason, aligned structures as filler within the lumen of the conduits are considered to be an important aspect for enhanced nerve regeneration as they support Schwann cell proliferation and alignment into Bands of Büngner like structures, axonal regrowth and finally bridging of the nerve cut ends. In else, the filler should be biodegradable, biocompatible, optimally porous, mechanically stable and more importantly, should impart topographical and biochemical cues for cellular attachment, growth and alignment,

respectively.¹⁹ Nerve growth factor (NGF) is a neurotrophic factor which provides biochemical cues to axons sprouting from the proximal stump. Different studies using tissue engineering scaffolds have shown the role of NGF in neuronal cell survival, growth, differentiation and enhancing nerve regeneration.^{20–23}

Over the last decade, cryogels, a form of hydrogels with interconnected pores fabricated using cryogelation technology have shown tremendous applications in the tissue engineering and regenerative medicine.^{24–28} We hypothesized that a 3D printed nerve guidance channel filled with aligned cryomatrix supplemented with NGF (aCG+NGF) will lead to efficient regeneration of the critical size nerve injuries. To augment this, in this work we fabricated and evaluated an aligned cryomatrix filled 3D printed guidance channels by a combinatorial approach, making use of stereolithography and cryogelation technology. We speculated that these 3D printed, aligned NGCs will mimic the endoneurial architecture and other aspects of physiological nerve. An in-vitro and in-vivo evaluation of the fabricated aligned NGCs with respect to the random filled matrix as well as hollow conduits was carried out to understand their potential in peripheral nerve regeneration. The fabricated NGCs showed enhanced neural regeneration in a critical size sciatic nerve defect in rats, and the regeneration potential was equivalent to that of autografts in terms of nerve physiology, morphology as well as cellular and structural aspects. To the authors' knowledge, this is the first study where 3D printed, aligned cryogel filled NGCs were fabricated and evaluated in-vitro and in-vivo for peripheral nerve regeneration. In else, this is the first report where a comparative study with different preclinically evaluated NGCs was done to demonstrate the importance of different cues for fabrication of NGCs for nerve regeneration.

2. Experimental Section

2.1. Synthesis and characterization of polycaprolactone (PCL) resin

In this study, four-armed, photocrosslinkable oligomer was synthesized from ϵ -caprolactone (Sigma-Aldrich, Germany) using pentaerythritol (10 mol-%, Fluka, Germany) as a co-initiator and stannous (II) 2-ethylhexanoate as an initiator (0.02 mol-%, Sigma-Aldrich, Germany). Oligomer was functionalized using excess of methacrylic anhydride (Sigma-Aldrich, Germany) to obtain reactive methacrylate groups. Methacrylation was continued at 60 °C for 24 h. After functionalization, the excess methacrylic anhydride was removed by precipitating in hexane. The residual hexane was removed under vacuum. Similar type of bulk ring-opening polymerization synthesis is described earlier using three-arm trimethylolpropane as co-initiator.^{29,30}

The average number molecular weight (M_n) and polydispersity (PDI) of synthesized and functionalized oligomer were determined using a Waters Associates system (Milford, MA, USA) equipped with a Waters 717Plus Satellite autosampler, a Waters 510 HPLC solvent pump, four linear PL gel columns (104, 105, 103, and 100 Å) connected in series, and a Waters 2414 differential refractometer. M_n and PDI were determined against linear polystyrene standards at room temperature. Chloroform was used as the eluent and was delivered at a flow rate of 1 ml/min. Samples were dissolved in chloroform at a concentration of 10 ppm. The injection volume was 200 μ l.

The viscosity of the resin was investigated on AR G2 rheometer (TA Instruments Ltd, USA) using a 20 mm steel plate at a constant shear rate 0.28 s⁻¹. DSC analysis was done using DSC Q2000 (TA Instruments, Delaware, USA) under nitrogen atmosphere. Two heating scans were made (10 °C/min) from -90 °C to 85 °C with 1 minute stand at 200 °C and cooling at rate of -50 °C/min. The glass transition (T_g) was analyzed from second heating and melting temperature (T_m) from the first.

Prior to 3D-printing, resin was prepared by mixing PCL oligomer with photoinitiator camphorquinone (1% w/w) (97%, Sigma-Aldrich, Germany) and photocrosslinking accelerator

ethyl 4-dimethyl amino benzoate (1% w/w) (Sigma-Aldrich, Germany). Orasol orange G (0.2% w/w) (Ciba AG, Switzerland) was used as a dye to control penetration depth during printing process. After mixing with initiators and dye, the resin was kept at room temperature for 24 h to enable additives to dissolve into the PCL oligomer.

2.2. Design and fabrication of three dimensional (3D) printed structures using stereolithography

The nerve conduit tubes were designed in SolidWorks SP5.0 (Dassault Systèmes, Vélizy-Villacoublay, France), and converted into triangular mesh format for 3D printing. Conduit lengths were 1.9 cm, with 1.5 cm porous section length in the 4-pore configuration, i.e. 2 mm sleeve length on both sides.

An in-house constructed projection stereolithography (PSLA) system and software was used in the fabrication of three dimensional printed structures.³¹ Fabrications were carried out at wavelength 400-500 nm, light intensity of 5600 $\mu\text{W}/\text{cm}^2$ and layer thickness of 25 μm . Two types of structures were developed using PCL resin: 1) disc for cell material interaction studies, 2) hollow and multichannel nerve conduits for in-vivo nerve regeneration. To remove the uncured resin, the 3D printed structures were immersed in 2-propanol (AppliChem GmbH, Germany) for 4-5 days until they became completely transparent.

2.3. Fabrication of cryogel filled nerve conduits

The aligned and random NGCs were developed by synthesizing cryogels within the lumen of the hollow 3D printed nerve conduits. Low viscosity chitosan (1.2% w/v, Sigma-Aldrich, USA) dissolved in 2 % acetic acid and gelatin (6.4% w/v, Sigma-Aldrich, USA) (from cold water fish skin) dissolved in distilled water were mixed together and kept at 4 °C. Further, 3D printed hollow conduits of 1.9 cm length were fixed to a steel plate and insulated with styrofoam. For the formation of aligned channels using liquid nitrogen vapors, the steel plate was placed on a container containing liquid nitrogen. The cold chitosan-gelatin solution mixed with 1.5% v/v

glutaraldehyde as a crosslinker was filled inside the lumen of the hollow conduit. The polymeric solution was unidirectionally frozen using cold vapors in order to form ice crystals in one direction. The frozen structure was kept at -20 °C for 12- 15 h for crosslinking and completion of cryogelation. The random NGCs were synthesized by freezing the solution at -20 °C for 12-15 h. The cryogel filled conduits were thawed and dried to obtain nerve guidance channels. In a similar way, earlier also we have fabricated and characterized aligned cryogel filled polyurethane nerve conduits using unidirectional cryogelation technology.³²

2.4. Nerve growth factor (NGF) incorporation in fabricated nerve conduits

The nerve growth factor incorporated NGCs were fabricated by adsorbing the growth factor on the dried guidance channels. Briefly, NGF (5 µg/ml) was mixed with BSA (0.1%) in a ratio of 1:160. NGF-BSA solution (10 µl) was injected in the lumen from both ends, filling the NGCs for uniform distribution. The NGCs were further incubated at 4 °C for 24 h for adsorption of the growth factor.

2.5. Characterization of the fabricated nerve conduits

The morphological analysis of the fabricated nerve conduits and cryogel filled nerve conduit was done using scanning electron microscopy (FEI Quanta 200). To study the surface hydrophilicity of the fabricated PCL discs, the water contact was measured using a contact angle goniometer (Dataphysics OCA 35, Germany) by the sessile drop method. The morphological properties of the fabricated guidance channels were determined by SEM analysis. The horizontal and vertical sections of the aligned cryogel filled conduits were imaged. The samples were gold coated using a sputter gold coater machine (Vacuum Tech, Bangalore, India) for 90 s and observed in SEM (FEI Quanta 200) at an accelerating voltage of 12.5 kV. Further, the dye flow test was performed to show the pore connectivity of the 4-Pore multichannel conduit. The mechanical properties of the 3D printed aCG NGCs was analyzed by mechanical testing system (Instron 1195). Micro-CT analysis was carried out at

energy settings of 35 kV and 216 μ A with 450 ms exposure at a resolution of 15 μ m (SkyScan1172, Bruker, Belgium).

2.6. In-vitro NGF release assay

To determine the in-vitro release kinetics of NGF from NGCs, the samples were incubated in 200 μ l phosphate buffered saline (PBS, pH 7.4) in incubator at 37 °C with gentle shaking. At regular time intervals for a period of 15 days, 100 μ l of the sample was collected and replaced with same amount of PBS. The samples were kept at -20 °C until analysis. The released NGF from the samples was detected by mouse beta-NGF ELISA kit (RayBio®).

2.7. In-vitro cell culture using neuronal cell line

The cell culture studies were performed on the PCL discs, aligned and random cryogels using Neuro2a neuroblastoma cells. The Neuro2a cells were procured from (NCCS, Pune, India) and cultured in high glucose DMEM supplemented with 10% (v/v) fetal bovine serum, 100 U/ml penicillin and 100 U/ml streptomycin at 37 °C in a 5% CO₂ atmosphere. The PCL discs and cryogels were sterilized using ethanol gradient (20% - 100%) for 15-30 min and then washed three times with phosphate-buffered saline (PBS). Subsequently, the Neuro2a cells were seeded on the PCL discs (8 mm diameter) and 48 well tissue culture plate (TCP) as control at a density of 5×10^4 cells/disc. The metabolic activity of Neuro2a cells was measured using MTT assay at different time points for a period of 7 days. On the aCG and rCG NGCs (1.5 mm diameter and 2 mm height), the Neuro2a cells were seeded at a density of 5×10^4 cells/NGC. As a control 96 well tissue culture plate (TCP) was used. The metabolic activity was measured using MTT assay for a period of 10 days. After 5 days of culture, the samples were fixed in 4% PFA for nuclear and cytoskeleton staining.

2.8. Surgical procedures

The surgical and implantation procedures were approved under the institutional animal ethical committee. Adult female Wistar rats weighing 250-300 g were randomly divided into 10

groups having 6 animals per group and 5 animals in sham control. In this work, neurotmesis model in sciatic nerve with 15 mm critical size defect was created and further studied for nerve regeneration. The different experimental groups of the study are mentioned in **Table 1**. Briefly, sciatic nerve surgery was performed on the rat right hind limb by anesthetizing them using isoflurane (2-4%). Sciatic nerve was exposed by making an incision from the right sciatic notch to distal thigh and transected creating a gap of 15 mm, which was bridged using different nerve guidance channels except negative control. In sham control, sciatic nerve was only exposed by detaching from the nearby tissue without damaging the nerve tissue. For autografts group, sciatic nerve was transected and sutured in reversed direction. For all the experimental groups, nerve endings were sutured using 10-0 resorbable sutures (Ethicon), and the muscle pouch was sutured back with 5-0 resorbable sutures (Ethicon). The outer skin was sutured by over and over using 5-0 resorbable sutures (Ethicon). All the animals except sham control received a daily dose of 12.5 mg/kg of tramadol for an initial 1 week for pain management. The animals were housed under standard conditions with 12 h light and dark with free access to food and water.

2.9. Functionality assessment of regenerated sciatic nerve

After surgery, the functional improvement of the nerve was evaluated by performing electrophysiology testing. For the analysis, electromyogram (EMG) machine (Nicolet Viking Quest) was used. Nerve conduction velocity (NCV) and compound muscle action potential (CMAP) were recorded for all animals from the experimental groups after 8, 12 and 16 weeks' of surgery. Briefly, the animals were anesthetized using isoflurane (2-4%), and the surgery portion of the right hind limb was shaved. The stimulating electrode was placed near the regenerated nerve and a recording electrode was placed at the gastrocnemius muscle. A reference electrode was placed between the stimulating and recording electrode and the ground electrode was placed at the tail. The nerve was stimulated at the proximal and distal end of the

implant. The distance between both the stimulated points was measured to calculate the NCV. The peak amplitude values of the CMAP were calculated.

2.10. Walking track analysis

To evaluate functional recovery after surgery, walking track analysis was carried out on completion of 4, 8, 12 and 16 weeks'. Briefly, a wooden walking alley with dimensions 1 m x 15 cm having a black box at the end was used in the analysis. A white sheet of paper was placed in the walking alley. The hind feet were dipped in a blue color dye, and animals were allowed to walk along the track. Sciatic nerve functional index (SFI) was calculated according to the following formula:

$$\text{SFI} = -38.3(\text{EPL-NPL})/\text{NPL} + 109.5(\text{ETS-NTS})/\text{NTS} + 13.3(\text{EIT-NIT})/\text{NIT}$$
 where,

PL, TS and IT represent paw length, toe spread length and intermediary toe spread length, respectively. E refers to experimental and N refers to normal for all the groups.^{33,34}

A walking aisle made of glass equipped with a video making system having dimensions of 80 cm x 6 cm x 12 cm was used for making videos of the rats from all the groups as previously mentioned.³⁵ A mirror was placed at 45° underneath the walking passage. The animals were permitted to walk freely on the track. The mirror reflected the image of the rat paws, and the video was recorded using a digital camera.

2.11. Histological and morphological assessment of regenerated sciatic nerve

The implanted nerve guidance channels isolated after 16 weeks' of surgery were immediately fixed in 4% PFA (paraformaldehyde) at 4 °C for 48 h. For Hematoxylin and Eosin (H&E) staining, regenerated sciatic nerve sections of 2 mm length were taken from each of the distal, proximal and middle segments. The samples were dehydrated in ethyl alcohol and then treated in xylene. Further, the segments were embedded in paraffin wax and cut into 7 µm thick transverse sections for H&E staining. Toluidine blue staining was performed on the middle sections of the regenerated nerve. Briefly, the PFA fixed samples were post fixed with 2%

osmium tetroxide for 2 h at room temperature (RT). After PBS washing, the samples were embedded in paraffin wax and sectioned as discussed earlier. The sections were stained with toluidine blue (1%) at 80 °C for 30-40 s. The H&E and toluidine blue light microscopic images were taken using microscope (Leica DM 2500). Morphometric analysis of regenerated axons was carried out using ImageJ software (NIH, USA).

2.12. Immunohistochemistry analysis

Immunostaining was performed on the middle segment of nerve grafts for NF-200 (1:50, Santa Cruz) and S-100 (1:50, Santa Cruz) markers. In brief, the antigen retrieval was done in sodium citrate buffer at 95 °C for 20-25 min. The non-specific antigens were blocked using 1% BSA. The sections were incubated with primary antibody for overnight at 4 °C. After washing, the sections were stained with FITC labelled secondary antibody (1:200, Invitrogen) for 2 h at RT. For counterstaining, the sections were incubated with propidium iodide for 10 min at RT. After mounting, the images were captured using LSM780NLO, Carl Zeiss GmbH confocal microscope. The quantification of the positive area was done using ImageJ software (NIH, USA).

2.13. Muscle weight ratio and muscle fiber analysis

After 16 weeks' of surgery, gastrocnemius muscle, the main target of the sciatic nerve was isolated from both the hind limbs of the rats. Moist weight ratio of muscle from the experimental leg to the contralateral leg was calculated immediately after the rats were sacrificed.³⁶ Additionally, to determine the muscle fiber diameter and morphology, the muscles were fixed using 4% PFA overnight at 4 °C like nerve samples as discussed earlier. Transverse sections of the paraffin wax embedded muscle samples were obtained using the microtome (Thermo Fisher Scientific) for H&E and Masson's trichrome staining. Further, the light microscopic images were taken using a digital camera (Nikon, Japan) from random portions of the stained sections. The muscle fiber diameters and the area of muscle per region of interest

were quantitatively analyzed for all the experimental groups. For each group, 5 Masson's trichrome stained sections were imaged and 4 random portions from each section were analyzed to calculate muscle fiber diameters and the area of muscle per region of interest using ImageJ software.

2.14. Statistical analysis

All the in-vitro experiments were carried out in triplicate keeping the minimum sample size of $n = 3$ and the quantitative experiments are expressed as mean \pm standard deviation. All the analysis was carried out using GraphPad Prism 5 using 2 tailed student's t-test and one way Anova tests. The p value of less than 0.05 was considered statistically significant.

2.15. Animal ethics statement

All the animal experiments were performed under the guidelines of the Institute Animal Ethics Committee (IAEC) using the approval numbers IITK/IAEC/2014/1019, IITK/IAEC/1023 and IITK/IAEC/1024. All the animals were housed in standard conditions with free access to feed and water. The animals were housed in cages with regulated temperature, light and humidity.

3. Results and Discussion

3.1. Synthesis and characterization of polycaprolactone (PCL)

Functionalized, photocrosslinkable polycaprolactone (PCL) was chosen as the oligomer due to its beneficial properties, such as 3D-printability and biocompatibility. Low molecular weight PCL oligomers have low viscosity, which enables the use of the oligomer in projection stereolithography (PSLA) without any added solvent. In our previous studies, three-armed methacrylated PCL oligomer has shown biocompatibility with fibroblast cells.^{29,37} In addition, thermoplastic PCL has been used successfully as a nerve conduit material in in-vivo nerve regeneration studies.^{38,39}

The synthesis reaction was monitored, and the structure of the oligomer was determined using a Bruker Ultrashield 400 Hz NMR spectrometer (Billerica, MA, USA). Samples (5 mg) for ^1H measurements were dissolved in 0.5 ml d-chloroform (99.8 % deuteration). The monomer conversion was complete as no monomer peak (2.66 ppm) was observed in the ^1H -NMR spectrographs (**Figure 1a**). The methacrylation was complete, as OH end groups (peaks 3.65 ppm and 3.50 ppm) were not observed (**Figure 1b**). The crosslinkability of the PCL resin was studied with a gel content analysis reaching a value of 99.8%, which confirms the high functionalization degree and reactivity of oligomer. The M_n on the functionalized oligomer was measured to be 3000 g/mol and PDI 1.2. The T_g was -60°C for oligomer and -61°C for printed sample. Oligomer had the melting temperature at 18°C , whereas no melting was observed for the printed PCL samples. Stereolithography requires low viscosity liquid resin to allow accurate preparation of the manufactured part.^{29,40} Previously, it has been reported that the resin should have viscosity of less than $10\text{Pa}\cdot\text{s}$ ⁴¹, however resins with higher viscosities have been used successfully.^{40,42} The PCL resin showed viscosity of $8\text{Pa}\cdot\text{s}$ at room temperature. The viscosity of functionalized PCL oligomer was suitable for the PSLA used in this study.

3.2. Fabrication and characterization of 3D printed NGCs

The hollow and multichannel NGCs with optimized parameters were fabricated to ensure its mechanical stability and ease in handling during surgery. **Figure 1c, 1d** represents axial views of the tube design with (a) hollow and (b) 4-pore configuration. The dimensions of the designed NGCs were made to mimic the physiological dimensions of the rat sciatic nerve, which ranges from 1.5-2 mm in diameter. The length of the nerve conduits was 1.9 cm and the inner diameter of 1.5 mm, with a sleeve length of 2 mm on both the ends to bridge a 15 mm nerve injury gap (**Figure S1**). The sleeves at the ends of the conduit provide an advantage of inserting nerve stem inside the conduit during suturing of the damaged nerve. In case of multichannel nerve conduits, four pores were developed during its fabrication with a diameter of 500 microns each

to mimic the endoneurial structure of the native nerve. Multichannel nerve conduits using electrospinning and stereolithography technique have been fabricated previously to mimic the natural nerve architecture.^{43,44} Previously, microstereolithography printed hollow nerve guidance conduits with aligned grooves were fabricated and evaluated in a 3 mm long non-critical size injury.¹⁶ Next, for fabrication of aligned NGC (aCG), we synthesized a unidirectionally oriented cryomatrix inside the lumen of the hollow conduit. In our previous study, we designed and fabricated aligned CG cryogel matrix using different freezing temperatures, polymer and crosslinker concentrations. We showed that the fabricated cryogels using CG concentration (7.6% w/v) and crosslinker concentration (1.5% v/v), frozen unidirectionally using liquid nitrogen vapors have optimum parameters in terms of pore size and pore alignment to be used as filler for NGC.³² Similarly, random cryomatrix was fabricated inside 3D printed conduits to get random NGC (rCG). Chitosan and gelatin are biocompatible and biodegradable polymers known to support neural cell adherence, growth and proliferation.¹⁹ Aligned 3D scaffolds allow SC migration to form longitudinally arranged column like structures, resembling Bands of Büngner for efficient nerve regeneration.⁴⁵ Aligned CG cryogel matrix inside aCG could provide topographical cues to the migrating and proliferating SCs after nerve injury. The fabricated hollow and cryogel filled NGCs were characterized for morphological and mechanical properties. The ideal NGCs should have suitable porosity, good mechanical strength and the lumen should be aligned in nature.⁴⁶ The fabricated 3D printed nerve conduit has an open pore structure throughout its lumen. The digital images of the hollow and multichannel conduits are represented in **Figure S1**. The presence of open pores in the 4-Pore multichannel conduit length was determined by dye flow test. The dye was observed to flow from one end to another without any obstruction (**Figure S1**), which is important to avoid any hindrance in the nerve tissue growth. The inner diameter and wall thickness of the 3D printed PCL nerve conduits were 1.45 ± 0.05 mm and 350 μ m,

respectively (**Figure 1e**). The inner diameter of the NGCs should match to the diameter of the injured nerve for the proper placement of the damaged nerve ends within the NGCs allowing regeneration. The fabricated 4-Pore multichannel conduits have 4-Pores with a diameter around $400\pm 90\text{ }\mu\text{m}$ as represented in the SEM image (**Figure 1f**). The transverse and longitudinal sections of the cryogel incorporated nerve conduits indicated that the porous cryogel inside the lumen of conduit was well integrated. This is important for mechanical stability and proper growth of the axons inside the aligned NGCs. Moreover, SEM micrographs revealed that the pores are open and aligned in nature with an average pore diameter of $50\text{ }\mu\text{m}$ (**Figure 1g, 1h**) which is optimal for Schwann cells migration and alignment.⁴⁵ The SEM micrograph of rCG represented random porous cryogel matrix in the lumen of the NGC (**Figure 1i**). Further, Micro-CT analysis also showed the filamentous architecture of the aligned cryogel matrix inside the NGCs (**Figure 1j**). The contact angle of the PCL discs was 54.95° which is suitable for cell adherence (**Figure 1k**). It has been shown that the contact angle of the material in the range of 40° to 80° is best suited for cell adherence.⁴⁷ The tensile modulus for aCG, rCG, HC and 4-Pore NGCs were $180\pm 10\text{ KPa}$, $140.03\pm 4.73\text{ KPa}$, $93.07\pm 2.83\text{ KPa}$ and $168.39\pm 3.35\text{ KPa}$ respectively as represented in (**Figure 1l**). Among all the NGCs, lowest tensile modulus ($93.07\pm 2.83\text{ KPa}$) was obtained for hollow conduits (HC). As the hollow conduit was filled with porous matrix (rCG), there was a steep increase in the tensile modulus as the filler matrix will provide more resistance to elongation leading to increase in the modulus ($140.03\pm 4.73\text{ KPa}$). Moreover, aligned matrix due to unidirectional porous architecture resists any deformation more strongly as compared to random matrix resulting in increased modulus of aCG ($180\pm 10\text{ KPa}$) as compared to rCG. In case of 4-Pore NGCs, higher tensile modulus ($168.39\pm 3.35\text{ KPa}$) was obtained, that may be attributed to their more solid structure as compared to that of hollow conduits. Further the conduits are flexible in nature and can be bent easily which is important to avoid any mechanical injury both to the surrounding tissue and the

regenerating nerve tissue. Thus, the aligned nerve guidance channel has desired optimal properties, suitable for peripheral nerve regeneration.

The NGF release kinetics from the NGCs was determined by ELISA assay for a period of 15 days. Sustained release of the growth factor was obtained from all the NGF adsorbed NGCs as represented in **Figure 1m**. Similar type of release pattern was obtained for all the NGCs with no significant differences among the groups. As determined by the ELISA assay, approximately 45%-50% NGF was released in the initial 3 days, indicating its burst release from the NGCs. Further, 15%-20% NGF was released, leading to 60%-70% of the total NGF released in the 1st week. Subsequently, at the end of 2nd week almost 75%-80% of the total NGF was released from the NGCs. Since the growth factor was loaded on to the NGCs by the simple adsorption method, therefore there was no physical resistance for the release of the NGF.

To evaluate the biological behavior of the fabricated NGCs, cell-material interaction was studied by culturing Neuro2a cells on 3D printed PCL discs, aligned and random NGCs. The photocured cylindrical PCL discs were 8 mm in diameter and 2 mm in height for performing in-vitro cell material interaction studies. The cellular metabolic activity and thus viability was evaluated by MTT assay for a period of 7 days (**Figure 2a**). Cell growth on PCL discs was comparable to that of the TCP (tissue culture plate) demonstrating that the 3D printed PCL discs are non-toxic for cell growth. To further analyze the cell adhesion and proliferation, SEM imaging of the cultured cells on PCL discs was done at day 5. The representative images showed that Neuro2a cells are well adhered on PCL discs (**Figure 2b**). This was also confirmed by fluorescent imaging for DAPI (blue, nuclear stain), and phalloidin-FITC (green, cytoskeleton stain) showing the uniform distribution of cells on the PCL discs with the extended morphology of cytoskeleton (**Figure 2c**). Collectively, these results specified that PCL material is not cytotoxic and supported neuronal cell adherence and proliferation. The

cellular metabolic activity on aCG and rCG NGCs was analyzed for a period of 10 days by MTT assay (**Figure 2d**). The MTT data indicated high proliferation rate of Neuro2a cells on both aCG and rCG NGCs. This demonstrated that the synthesized NGCs are biocompatible in nature showing high cellular proliferation. Further, to analyze the effect of pore architecture in controlling cellular alignment, SYTOX Green fluorescent staining was performed on both aligned and random cryogels (**Figure 2e, 2f**). The fluorescent images demonstrated that cells migrated in aligned fashion on aligned scaffolds following the unidirectional pores whereas on random cryogels, cells migrated in an arbitrary fashion. Also, the cells infiltrated deep into the aligned scaffolds following the aligned channels as represented in **Figure 2g**. Taken together, these results demonstrated the importance of aligned porous cryogels in controlling cellular alignment. Similarly, in our previous study, we have shown the in-vitro culture of dorsal root ganglion explants on aligned cryogels, where, the DRG Schwann cells and neurons proliferated, migrated and aligned along the unidirectional porous architecture of the aligned scaffolds.³²

3.2. In-vivo sciatic nerve regeneration

After establishing the in-vitro feasibility of aligned nerve guidance channels for nerve regeneration, we investigated the potential of this scaffold in in-vivo nerve regeneration. To augment this, NGCs were implanted in a critical size defect in rat sciatic nerve injury model (**Figure 3 a-f**). All the animals survived the experimental period and no sign of infection was observed. The animals were continuously monitored for functional recovery through electrophysiology and walking track analysis. After 16 weeks' of surgery, the animals were sacrificed, samples were harvested and analyzed for nerve regeneration.

3.3. Functionality assessment of regenerated sciatic nerve

3.3.1. Electrophysiology

Electrophysiological properties of the regenerated sciatic nerve were determined to analyze the functional reinnervation after sciatic nerve injury. Nerve conduction velocity (NCV) and compound muscle action potential (CMAP) values were calculated at postoperative intervals of 8, 12 and 16 weeks' for all the experimental groups (**Table 2**). The NCV and CMAP values for the nerve guide implanted groups showed improvement over the period of 16 weeks' (**Figure 3g, 3h**). The measurement of NCV gives insight into the conducting properties of the regenerated sciatic nerve. The CMAP recordings for all the experimental groups after 16 weeks' post operatively are represented in (**Figure S2**). The sham control group exhibited normal NCV and CMAP values of 59.8 ± 1.64 m/s and 17.82 ± 1.01 mV, respectively, which remains approximately similar at all the measured time intervals. After 8 weeks' post implantation, maximum NCV and CMAP values were observed for autografts group. For aCG+NGF implanted group; NCV values were lower than autografts group; however, CMAP values were comparable to that of the autografts. The aCG and rCG+NGF groups showed non-significant differences in NCV and CMAP values, but were significantly higher than that of rCG and HC+NGF group. Moreover, rCG and HC+NGF group has substantially higher NCV values than HC group. These results indicate towards the important role of topographical and biochemical cues in enhancing electrophysiological parameters. 4P+NGF and 4P implanted group does not show any significant improvement in NCV and CMAP values, and were lower than that of HC as well as other groups.

At 12 and 16 weeks' post implantation, the NCV and CMAP values increased for all groups (**Figure 3g, 3h**). However, it was interesting to observe no significant difference between the values of autografts and aCG+NGF group ($p > 0.05$). Moreover, with respect to other groups, the NCV and CMAP for both aCG+NGF and autografts were significantly higher. There was a notable difference in both NCV and CMAP between aCG and aCG+NGF groups, thus indicating an essential role of NGF in nerve regeneration. Among aCG and rCG+NGF, a non-

significant difference was observed in the physiological parameters at 12 weeks ($p>0.05$), however, a significant difference after 16 weeks' post-implantation ($p\leq0.05$) indicated towards better regeneration capability in aligned cryogel filled than that of random cryogel filled NGCs. For rCG+NGF and HC+NGF groups, the electrophysiological parameters were significantly higher for rCG+NGF group after 12 and 16 weeks, elucidating that matrix filled NGCs show enhanced nerve growth than hollow nerve conduits. Among rCG and HC+NGF groups, NCV and CMAP values does not show any differences ($p>0.05$) at 12 and 16 weeks, however these values were higher than HC group at both the time intervals, indicating the role of filler matrix and NGF respectively, in enhancing nerve regeneration. We observed a combined effect of filler matrix, topographical and biochemical cues provided by the nerve guidance channel in enhancing nerve electrophysiology, hence regeneration. The multi-channel 4-Pore implanted groups does not show any significant improvement in electrophysiological parameters of NCV and CMAP over the period of 16 weeks. We could not observe any peaks for the negative control group.

Maximum NCV and CMAP values obtained in aCG+NGF group may be attributed to the topographical cues provided by aligned CG cryogel filler and biochemical cues provided by NGF. Enhancement in NCV and CMAP values indicated towards an increased degree of remyelination of the regenerated nerve after neurotmesis. The aligned cryogel filler may have resulted into more Schwann cell migration and adherence, and further axonal regeneration in comparison to random cryogel filler or hollow conduit leading to increase in NCV as well as CMAP. These results also demonstrate that the aCG guidance channels may not only lead to efficient nerve regeneration, but also preserved the muscle physiology necessary for an efficient clinical outcome.

3.3.2. Walking track analysis

The sciatic nerve functional index, an important functional recovery outcome was calculated by walking track analysis to determine the recovery of the locomotion after nerve injury postoperative 4, 8, 12 and 16 weeks'. The sciatic nerve is the longest single nerve in the body which bifurcates into two different nerves, which controls the sensation and motor functions of the foot. Thus, for practical functional recovery after nerve injury, it is necessary to regain the motor activities. For SFI values, -100 represents complete damage to the nerve, and 0 represents the normal functional nerve. After 4 weeks', the SFI values does not show any significant improvement and were approximately similar for all the experimental groups (**Figure 3i**). After 8 weeks' post-implantation, the SFI values have improved in all the implanted groups with significant differences in comparison to that of negative control group. Significant improvement in SFI after NGCs implantation became more evident and noticeable after 12 weeks'. The SFI values for autografts and aCG+NGF implanted group does not show any significant difference ($p>0.05$) and was -58.90 ± 4.01 and -60.21 ± 1.65 , respectively. This implies that the aCG+NGF NGCs is showing equivalent functional recovery to that of autografts. Moreover, aCG+NGF group has SFI value more than the aCG group (-65.86 ± 1.18 ; $p\leq0.01$) showing enhanced improvement in functionality by using NGF. Between aligned aCG and random rCG, the aCG group has significantly higher SFI value than rCG. This again indicates towards an important role of alignment, in improving the nerve regeneration and thus functionality of the innervated tissue in comparison to random NGCs. The trend remained similar; however, the values became more prominent after 16 weeks' of surgery. The SFI value for aCG+NGF implanted group (-44.53 ± 1.90) was statistically equal to that of autografts (-44.43 ± 3.45), showing maximum recovery in functionality in comparison to other implanted groups. The SFI values for aCG, rCG and HC were -52.31 ± 1.60 , -59.23 ± 1.21 and -65.77 ± 0.93 , respectively having significant differences between them. In 4-Pore implanted groups, we could not find any significant improvement in SFI over a period of 16 weeks. These results

further indicate towards a significant role of aligned cryogel filler over random cryogel filler in regaining the nerve functionality after critical injury. Moreover, lumen filled NGCs performed better than the hollow conduits as they provide matrix for native cells attachment, proliferation and directional growth. Previous studies have also shown that cellular behavior was directly influenced by the presence of microenvironment within the nerve conduits and enhanced nerve functionality was obtained in filled conduits in comparison to the hollow nerve conduits.⁴⁸ The functional recovery can also be seen by visual observation of the toe spreading (**Figure 3j-l**), which was significant in case of aCG+NGF implanted group compared to that of autografts. No such toe spreading was observed for the negative control group. The functional recovery can also be observed in the representative videos for gait pattern (**Supporting videos SV1, SV2 and SV3**).

3.4. Histological and morphological assessment of regenerated sciatic nerve

To assess the histological improvements of the regenerated nerve; hematoxylin and eosin (H&E), toluidine blue and immunofluorescence staining were carried out after 16 weeks' post implantation. For H&E staining, proximal, middle and distal portions of the implanted NGCs from all the experimental groups were analyzed to determine the regenerated nerve morphology. As a general observation, all the NGCs demonstrated nerve regeneration (**Figure 4**). At the proximal end, healthy nerve fibers were observed in all the groups, indicating that the nerves had regenerated from the proximal end to their respective distal end. From the microscopic observations of the middle sections, in comparison to the CG cryogel filled guidance channels the regenerated sciatic nerve has the smallest diameter in hollow conduits. Whereas, all the cryogel incorporated guidance channels performed better than hollow conduits. For successful axonal regeneration, NGCs should provide cellular adherence, topographical and biochemical cues to the sprouting axons. The filler cryogel contains chitosan, which is a natural copolymer of D-Glucosamine and N-acetyl-D-Glucosamine known

to enhance peripheral nerve regeneration.⁴⁹ Also, the degradation products of chitosan induce the proliferation of SCs during nerve regeneration.⁵⁰ Moreover, chitosan along with gelatin enhance SC adhesion and migration, which further directs axonal growth resulting in better regeneration in CG cryogel filled conduits. Among the cryogel filled NGCs, aCG showed significantly better regeneration than the rCG. Topographical cues in terms of pore alignment, which mimics the physiological nerve architecture are known to enhance nerve regeneration rate by providing guidance to the migrating and proliferating neural cells. These topographical cues help SCs to form Bands of Büngner like structure that provide guidance to the sprouting axons from proximal stump.¹⁸ Aligned channels present in the aCG provided topographical cues for SCs alignment, directing sprouting axons from proximal to distal end. Also the aligned NGCs provided an obstacle free path to growing axons resulting in efficient nerve regeneration than random NGCs. Among all the NGC implanted groups the aCG+NGF group showed the maximum area and density of the regenerated nerve fibers equivalent to that of the autografts group (**Figure 4b, 4c**). The quantitative estimation of the area of the regenerated nerve also showed that there is non-significant difference between aCG+NGF and autografts ($p > 0.05$), which is significantly higher than that of HC group (**Figure S3A**). The aCG+NGF showed enhanced nerve regeneration in comparison to aCG only, depicting an essential role of NGF in nerve regeneration (**Figure 4c, 4d**). Bioactive molecules, particularly nerve growth factor (NGF) enhances nerve regeneration by inducing the expression of cytoskeletal proteins such as alpha tubulin, thus playing an important role in the extension and maintenance of the axonal growth cone.⁵¹ Similar results were obtained between rCG+NGF and rCG group (**Figure 4e, 4f**), where NGF incorporated group has shown better regeneration in terms of area and density of the regenerated fibers. In fact, the presence of NGF has improved nerve regeneration in the HC+NGF group as well (**Figure 4g, 4h**) with respect to HC only. In case of 4P+NGF and 4P NGCs substantial nerve regeneration was not observed. It may be due to the non porous walls

of the 4-Pore multichannel conduits, which obstructed the nerve tissue growth. Very few nerve fibers with small diameter were noticed (**Figure 4i, 4j**) and there were lot of variations among the different animals in each group. At the distal end, a certain degree of healthy nerve fibers were observed in all the implanted groups. Although the density of the nerve fibers was less as compared to the proximal and middle section as observed in **Figure 4**. The filler cryogel in case of random as well as aligned NGCs has almost degraded within 16 weeks with traces of cryogel observed in histological images. This is important for the efficient nerve regeneration as the degradable filler will pave way for the growing axons as the regeneration occurs over time. Also, the degradation rate was comparable to that of the axonal regeneration as most of the filler cryogel has degraded as observed by few remaining traces of cryogel. We speculate that one of the reasons for inefficient regeneration in 4-Pore implanted groups is the slow degradation of the conduit, which could have led to obstacle axon growth. Similarly, in previous studies it has been shown that multi-lumen conduits cause interference for regrowing axons, thus inhibiting successful nerve regeneration.¹⁷

Peripheral nerve regeneration is governed by SCs, the key players involved throughout the regeneration process. Following nerve injury SCs undergo de-differentiation and then guide the growing nerve fibers across the nerve bridge to connect the severed stumps. To evaluate the repair of nerve at the cellular level, immunological staining of neurofilament marker NF-200 and SCs specific marker S-100 was carried out. NF-200, an intermediate filament present in the mature neurons provides a structural support and helps in the axonal regeneration. S-100 depicts the proliferation and maturation of SCs. Immunological staining of the middle sections of the regenerated nerve demonstrated the expression of NF-200 (**Figure 5**) and S-100 (**Figure 6**) markers in the implanted groups confirming the presence of axons and the formation of myelin sheaths. However, there were variations in expression of markers in between the groups. The cryogel filled NGCs showed more expression of both markers in comparison to

1
2
3
4
5
6
7
8
9
10
11
12
13
14
15
16
17
18
19
20
21
22
23
24
25
26
27
28
29
30
31
32
33
34
35
36
37
38
39
40
41
42
43
44
45
46
47
48
49
50
51
52
53
54
55
56
57
58
59
60

hollow lumen NGCs. This was analysed by the quantitative estimation of the positive area for NF-200 and S-100 markers, which showed approximately equal expression for aCG+NGF and autografts, however, significantly higher than that of HC group (**Figure S3B, S3C**). In literature, it has also been shown that lumen filled NGC enhances the expression of such proteins and nerve regeneration in comparison to hollow conduits.⁵² In aCG+NGF group, the expression of both the marker proteins was more as compared to other implanted groups and is similar to that of the autograft. This further strengthened the result that the aligned cryogel have a beneficial effect in terms of NF-200 and S-100 expressions as compared to other experimental groups. Topographical cues assist the SCs to grow in a columnar fashion resembling the physiological architecture of the nerve. The pore size and pore alignment of the aCG NGCs provided topographical cues, specifically for SCs migration and alignment, which further supported and guided regenerating axons.

The conduction and functionality of the regenerated axons are dependent upon the extent of myelination. The myelin sheath around the axons is formed by the SCs, which undergo dedifferentiation and then proliferation to support axonal regeneration.⁵³ For the detailed analysis of the regenerated myelin sheath around the regenerated axons, toluidine blue staining of the middle sections was carried out. The myelination of the axons was observed in all the experimental groups except 4-Pore NGCs (**Figure 7 a-i**). The aCG+NGF and autograft groups showed a significant number of myelinated axons. On the contrary, the other groups showed relatively fewer numbers of myelinated axons. Moreover, the regenerated axons were growing in small clusters in autografts, aCG+NGF and aCG groups. This uniform distribution of axons mimics the physiological arrangement, a characteristic feature of a healthy nerve. Other studies have also shown that aligned longitudinal microstructures supports the cellular arrangement in clusters.⁵⁴ In the other cryogel filled groups such as rCG+NGF and rCG, few small clusters of cells can be observed, depicting the role of filler in enhancing axonal regeneration. This

1 attributed the fact that the aligned cryogel filled nerve guidance channels mimics the
2
3 physiological characteristics of the nerve and lead to enhanced regeneration after critical injury.
4
5 Morphometric analysis of the regenerated nerve in terms of the nerve diameter, axon diameter,
6
7 myelin sheath thickness, and axon density were calculated between the experimental groups
8
9
10
11
12 (Figure 8 a-d). The enlarged RGB toluidine blue stained image along with the description of
13
14 analysis of different parameters is represented in Figure S4. The statistical analysis depicted
15
16 that, the nerve diameter, axon diameter, myelin thickness and axon density were significantly
17
18 higher in aligned cryogel filled NGC as compared to random and hollow NGCs. The nerve
19
20 diameter of the regenerated fibers was comparable for the autografts, aCG+NGF and aCG
21
22 NGCs implanted groups ($p > 0.05$). However, it was significantly higher than the other
23
24 implanted groups ($p \leq 0.001$). Similar trend was observed in axon diameter, where, autografts,
25
26 aCG+NGF, aCG as well as rCG+NGF groups did not show any significant differences
27
28 ($p > 0.05$). Whereas, significant difference in axon diameter was observed in comparison to
29
30 other implanted groups ($p < 0.05$). The myelin thickness of the regenerated nerves was
31
32 maximum for the aCG+NGF group, similar to that of the autografts ($p > 0.05$), while it showed
33
34 significant differences in comparison to aCG and other groups ($p \leq 0.001$). This demonstrates
35
36 the effect of NGF as biochemical cue along with topographical cues in enhancing nerve
37
38 regeneration. Previous reports have also shown the role of exogeneously delivered NGF in
39
40 improving myelin sheath thickness of the regenerated nerve.⁵⁵ The axon density, which is the
41
42 number of axons per field of interest was higher in aCG+NGF group as compared to other
43
44 implanted NGCs ($p \leq 0.001$) but similar to that of autografts. All these results indicate a
45
46 combined role of the aligned filler matrix and biochemical cues inside conduit for efficient
47
48 regeneration at the cellular level. Further, it also depicts the fact that aligned cryogel filled
49
50 NGCs along with NGF results in comparatively better nerve regeneration than the random
51
52 cryogel filled and hollow NGCs.
53
54
55
56
57
58
59
60

3.5. Muscle weight ratio and muscle fiber analysis

After 16 weeks' of surgery, the functional recovery of the atrophied gastrocnemius muscle after neurotmesis was analyzed by isolating and analyzing the muscle weight ratio, Masson's trichrome and H&E staining. The gastrocnemius muscles from both the hind legs were isolated from all the experimental groups and the wet weight ratios of the experimental leg to the contralateral normal leg were calculated. Following nerve regeneration and innervation, the atrophied muscle recovered substantially as observed by the GM ratio for the implanted groups as compared to negative control groups (**Figure 9**). However, the values were considerably lower than the sham control group. The aCG+NGF and autograft group did not show any significant differences in GM ratio ($p>0.05$). However, there was a significant difference in the GM ratios of aCG+NGF in comparison to aCG revealing the effect of NGF in regaining muscle weight after injury. This effect on improving muscle weight was observed in other NGF incorporated experimental groups as well. Additionally, the GM ratio was higher for aCG than rCG+NGF and rCG revealing the effect of aligned channels over random channels in enhancing nerve regeneration and thus muscle reinnervation. Moreover, the rCG group has a significantly higher GM ratio than HC+NGF and HC groups showing the importance of cryogel filled guiding conduits above hollow conduits.

To evaluate the morphology of the atrophied gastrocnemius muscle Masson's trichrome and H&E staining was performed on the transverse muscle sections in all the experimental groups. The light microscopic images after Masson's trichrome staining showed the muscle fiber morphology in all groups with visible signs of muscle atrophy in hollow conduit and 4-Pore NGCs (**Figure 10**). Morphometric analysis for average cross-sectional area of muscle per region of interest and diameter of muscle fibers showed a similar trend like GM weight ratio analysis for all the experimental groups (**Figure 10l, 10m**). Average cross-sectional area and muscle fiber diameter were maximum for aCG+NGF and autografts groups in comparison to

all other experimental groups. Prominent muscle atrophy and reduction in muscle fibers was observed for the negative control group. Deposition of collagen fibers was observed in 4P+NGF, 4P and the negative control group in Masson's trichrome staining. This was further confirmed in H&E staining, where muscle atrophy followed by infiltration of inflammatory cells was observed in HC, 4-Pore NGCs and negative control group (**Figure 10**). The Masson's trichrome and H&E staining corroborated with the results of GM ratio. No significant muscle atrophy was observed for aCG+NGF and autografts group. All these results further strengthened the outcome of the 3D printed aligned cryogel filled NGCs in enhancing the regeneration of severely injured neurons. We believe that this will help in developing better strategies for development of the functionalized NGCs for efficient nerve regeneration.

4. Conclusion

In summary, the current study demonstrated the feasibility and application of a 3D printed aligned cryomatrix filled biomimetic NGCs in regeneration of critical sized nerve defects. The combination of different cues in a single device maximized the preclinical outcome of these biomimetic NGCs and could be promising for peripheral nerve regeneration. The developed NGCs take into account the clinically relevant requirements for a successful NGC by providing the topographical and biochemical cues in a single structure. Moreover the use of 3D printing makes this product a kind of advanced approach of personalized medicine for peripheral nerve repair and regeneration.

5. Acknowledgement

Funding received from Department of Biotechnology (DBT), Ministry of Science and Technology, Govt. of India (project # BT/PR13561/MED/32/392/2016) is duly acknowledged. We also acknowledge the funding received from Academy of Finland as mobility grant (decision No. 298568) to AK. AS, PAS, AKT, IQ would like to acknowledge IIT Kanpur for

fellowships for their PhD programme. Polymer synthesis and 3D printing made use of AALTO University Bioeconomy facilities. SA would like to acknowledge Jenny and Antti Wihuri foundation for providing funding for the project. We would like to acknowledge Pekka Lehtinen and Minna Malin from Aalto University for assisting in handling the 3D printer machine.

6. Author Contributions

AK and AS designed the whole study and experimental plan with inputs from JS and JP on 3D printing. SA synthesized and characterized the photocurable polycaprolactone and guided in printing the samples. EH has done the CAD designing of the 3D printed conduits. AS has fabricated the nerve guidance channels and carried out the material and in-vitro characterization. AS, AKT performed the animal surgery and implantation under supervision of AK. AS and IQ were responsible for overall animal care and maintenance. IQ has done the microCT analysis of the nerve guidance channels. AS performed the functionality tests and PAS performed the histology of the harvested samples and result analysis. AS and PAS wrote the initial draft of MS with review from AK. JS, JP reviewed overall MS.

7. Disclosure

The work reported here has duly been applied for provisional invention disclosure (Patent No. FI20185209; dated 06-03-2018).

8. Competing interests

The authors declare no competing financial interests.

Supporting Information

Video SV1: Video showing gait pattern of rat implanted with aCG+NGF NGCs.

Video SV2: Video showing gait pattern of rat implanted with autografts.

Video SV3: Video showing gait pattern of negative control group.

9. References

- (1) Ichihara, S.; Inada, Y.; Nakamura, T. Artificial Nerve Tubes and Their Application for Repair of Peripheral Nerve Injury: An Update of Current Concepts. *Injury* **2008**, *39*, 29–39.
- (2) Schmidt, C. E.; Leach, J. B. Neural Tissue Engineering: Strategies for Repair and Regeneration. *Annu. Rev. Biomed. Eng.* **2003**, *5* (1), 293–347.
- (3) Millesi, H. Techniques for Nerve Grafting. *Hand Clin.* **2000**, *16* (1), 73–91, viii.
- (4) Kehoe, S.; Zhang, X. F.; Boyd, D. FDA Approved Guidance Conduits and Wraps for Peripheral Nerve Injury: A Review of Materials and Efficacy. *Injury* **2012**, *43* (5), 553–572.
- (5) Deumens, R.; Bozkurt, A.; Meek, M. F.; Marcus, M. A. E.; Joosten, E. A. J.; Weis, J.; Brook, G. A. Repairing Injured Peripheral Nerves: Bridging the Gap. *Prog. Neurobiol.* **2010**, *92* (3), 245–276.
- (6) Wang, S.; Cai, L. Polymers for Fabricating Nerve Conduits. *Int. J. Polym. Sci.* **2010**, *2010*, 1–20.
- (7) Sarker, M.; Naghieh, S.; McInnes, A. D.; Schreyer, D. J.; Chen, X. Strategic Design and Fabrication of Nerve Guidance Conduits for Peripheral Nerve Regeneration. *Biotechnol. J.* **2018**, 1700635.
- (8) Matsumoto, K.; Ohnishi, K.; Kiyotani, T.; Sekine, T.; Ueda, H.; Nakamura, T.; Endo, K.; Shimizu, Y. Peripheral Nerve Regeneration across an 80-Mm Gap Bridged by a Polyglycolic Acid (PGA)-Collagen Tube Filled with Laminin-Coated Collagen Fibers:

- A Histological and Electrophysiological Evaluation of Regenerated Nerves. *Brain Res.* **2000**, *868* (2), 315–328.
- (9) Tonda-Turo, C.; Audisio, C.; Gnani, S.; Chiono, V.; Gentile, P.; Raimondo, S.; Geuna, S.; Perroteau, I.; Ciardelli, G. Porous Poly(ϵ -Caprolactone) Nerve Guide Filled with Porous Gelatin Matrix for Nerve Tissue Engineering. *Adv. Eng. Mater.* **2011**, *13* (5), B151–B164.
- (10) Ceballos, D.; Navarro, X.; Dubey, N.; Wendelschafer-Crabb, G.; Kennedy, W. R.; Tranquillo, R. T. Magnetically Aligned Collagen Gel Filling a Collagen Nerve Guide Improves Peripheral Nerve Regeneration. *Exp. Neurol.* **1999**, *158* (2), 290–300.
- (11) He, L.; Zhang, Y.; Zeng, C.; Ngiam, M.; Liao, S.; Quan, D.; Zeng, Y.; Lu, J.; Ramakrishna, S. Manufacture of PLGA Multiple-Channel Conduits with Precise Hierarchical Pore Architectures and *In Vitro/Vivo* Evaluation for Spinal Cord Injury. *Tissue Eng. Part C Methods* **2009**, *15* (2), 243–255.
- (12) Ao, Q.; Wang, A.; Cao, W.; Zhang, L.; Kong, L.; He, Q.; Gong, Y.; Zhang, X. Manufacture of Multimicrotubule Chitosan Nerve Conduits with Novel Molds and Characterization *In Vitro*. *J. Biomed. Mater. Res. Part A* **2006**, *77A* (1), 11–18.
- (13) Johnson, B. N.; Lancaster, K. Z.; Zhen, G.; He, J.; Gupta, M. K.; Kong, Y. L.; Engel, E. A.; Krick, K. D.; Ju, A.; Meng, F.; Enquist, L. W.; Jia, X.; McAlpine, M. C. 3D Printed Anatomical Nerve Regeneration Pathways. *Adv. Funct. Mater.* **2015**, *25* (39), 6205–6217.
- (14) Zhu, W.; Tringale, K. R.; Woller, S. A.; You, S.; Johnson, S.; Shen, H.; Schimelman, J.; Whitney, M.; Steinauer, J.; Xu, W.; Yaksh, T. L.; Nguyen, Q. T.; Chen, S. Rapid Continuous 3D Printing of Customizable Peripheral Nerve Guidance Conduits. *Mater.*

Today **2018**.

- (15) Gu, B. K.; Choi, D. J.; Park, S. J.; Kim, M. S.; Kang, C. M.; Kim, C.-H. 3-Dimensional Bioprinting for Tissue Engineering Applications. *Biomater. Res.* **2016**, *20* (1), 12.
- (16) Pateman, C. J.; Harding, A. J.; Glen, A.; Taylor, C. S.; Christmas, C. R.; Robinson, P. P.; Rimmer, S.; Boissonade, F. M.; Claeysens, F.; Haycock, J. W. Nerve Guides Manufactured from Photocurable Polymers to Aid Peripheral Nerve Repair. *Biomaterials* **2015**, *49*, 77–89.
- (17) Evangelista, M.; Perez, M.; Salibian, A.; Hassan, J.; Darcy, S.; Paydar, K.; Wicker, R.; Arcaute, K.; Mann, B.; Evans, G. Single-Lumen and Multi-Lumen Poly(Ethylene Glycol) Nerve Conduits Fabricated by Stereolithography for Peripheral Nerve Regeneration In Vivo. *J. Reconstr. Microsurg.* **2015**, *31* (5), 327–335.
- (18) Bozkurt, A.; Lassner, F.; O'Dey, D.; Deumens, R.; Böcker, A.; Schwendt, T.; Janzen, C.; Suschek, C. V.; Tolba, R.; Kobayashi, E.; Sellhaus, B.; Tholl, S.; Eummelen, L.; Schügner, F.; Olde Damink, L.; Weis, J.; Brook, G. A.; Pallua, N. The Role of Microstructured and Interconnected Pore Channels in a Collagen-Based Nerve Guide on Axonal Regeneration in Peripheral Nerves. *Biomaterials* **2012**, *33* (5), 1363–1375.
- (19) Chiono, V.; Tonda-Turo, C. Trends in the Design of Nerve Guidance Channels in Peripheral Nerve Tissue Engineering. *Prog. Neurobiol.* **2015**, *131*, 87–104.
- (20) Cao, X.; Shoichet, M. S. Investigating the Synergistic Effect of Combined Neurotrophic Factor Concentration Gradients to Guide Axonal Growth. *Neuroscience* **2003**, *122* (2), 381–389.
- (21) Belkas, J. S.; Shoichet, M. S.; Midha, R. Axonal Guidance Channels in Peripheral Nerve Regeneration. *Oper. Tech. Orthop.* **2004**, *14* (3), 190–198.

- (22) Oh, S. H.; Kang, J. G.; Kim, T. H.; Namgung, U.; Song, K. S.; Jeon, B. H.; Lee, J. H. Enhanced Peripheral Nerve Regeneration through Asymmetrically Porous Nerve Guide Conduit with Nerve Growth Factor Gradient. *J. Biomed. Mater. Res. Part A* **2018**, *106* (1), 52–64.
- (23) Yeh, C.-W.; Wang, L.-W.; Wu, H.-C.; Hsieh, Y.-K.; Wang, J.; Chen, M.-H.; Wang, T.-W. Development of Biomimetic Micro-Patterned Device Incorporated with Neurotrophic Gradient and Supportive Schwann Cells for the Applications in Neural Tissue Engineering. *Biofabrication* **2017**, *9* (1), 15024.
- (24) Kumar, A.; Srivastava, A. Cell Separation Using Cryogel-Based Affinity Chromatography. *Nat. Protoc.* **2010**, *5* (11), 1737–1747.
- (25) Vishnoi, T.; Kumar, A. Conducting Cryogel Scaffold as a Potential Biomaterial for Cell Stimulation and Proliferation. *J. Mater. Sci. Mater. Med.* **2013**, *24* (2), 447–459.
- (26) Kumari, J.; Karande, A. A.; Kumar, A. Combined Effect of Cryogel Matrix and Temperature-Reversible Soluble–Insoluble Polymer for the Development of in Vitro Human Liver Tissue. *ACS Appl. Mater. Interfaces* **2016**, *8* (1), 264–277.
- (27) Priya, S. G.; Gupta, A.; Jain, E.; Sarkar, J.; Damania, A.; Jagdale, P. R.; Chaudhari, B. P.; Gupta, K. C.; Kumar, A. Bilayer Cryogel Wound Dressing and Skin Regeneration Grafts for the Treatment of Acute Skin Wounds. *ACS Appl. Mater. Interfaces* **2016**, *8* (24), 15145–15159.
- (28) Damania, A.; Kumar, A.; Teotia, A. K.; Kimura, H.; Kamihira, M.; Ijima, H.; Sarin, S. K.; Kumar, A. Decellularized Liver Matrix-Modified Cryogel Scaffolds as Potential Hepatocyte Carriers in Bioartificial Liver Support Systems and Implantable Liver Constructs. *ACS Appl. Mater. Interfaces* **2018**, *10* (1), 114–126.

- (29) Elomaa, L.; Teixeira, S.; Hakala, R.; Korhonen, H.; Grijpma, D. W.; Seppälä, J. V. Preparation of Poly(ϵ -Caprolactone)-Based Tissue Engineering Scaffolds by Stereolithography. *Acta Biomater.* **2011**, 7 (11), 3850–3856.
- (30) Korhonen, H.; Helminen, A.; Seppälä, J. V. Synthesis of Polylactides in the Presence of Co-Initiators with Different Numbers of Hydroxyl Groups. *Polymer (Guildf)*. **2001**, 42 (18), 7541–7549.
- (31) Korhonen, H.; Sinh, L. H.; Luong, N. D.; Lehtinen, P.; Verho, T.; Partanen, J.; Seppälä, J. Fabrication of Graphene-Based 3D Structures by Stereolithography. *Phys. status solidi* **2016**, 213 (4), 982–985.
- (32) Singh, A.; Shiekh, P. A.; Das, M.; Seppälä, J.; Kumar, A. Aligned Chitosan-Gelatin Cryogel-Filled Polyurethane Nerve Guidance Channel for Neural Tissue Engineering: Fabrication, Characterization, and In Vitro Evaluation. *Biomacromolecules* **2018**, acs.biomac.8b01308.
- (33) Zhong, J.; Dietzel, I. D.; Wahle, P.; Kopf, M.; Heumann, R. Sensory Impairments and Delayed Regeneration of Sensory Axons in Interleukin-6-Deficient Mice. *J. Neurosci.* **1999**, 19 (11), 4305–4313.
- (34) Sarikcioglu, L.; Demirel, B. M.; Utuk, A. Walking Track Analysis: An Assessment Method for Functional Recovery after Sciatic Nerve Injury in the Rat. *Folia Morphol. (Warsz)*. **2009**, 68 (1), 1–7.
- (35) Hsieh, T.-H.; Chen, J.-J. J.; Chen, L.-H.; Chiang, P.-T.; Lee, H.-Y. Time-Course Gait Analysis of Hemiparkinsonian Rats Following 6-Hydroxydopamine Lesion. *Behav. Brain Res.* **2011**, 222 (1), 1–9.
- (36) Liu, Y.; Liu, Q.; Wang, Y. Ganglioside Promotes the Bridging of Sciatic Nerve Defects

- in Cryopreserved Peripheral Nerve Allografts. *Neural Regen. Res.* **2014**, *9* (20), 1820.
- (37) Elomaa, L.; Kokkari, A.; Närhi, T.; Seppälä, J. V. Porous 3D Modeled Scaffolds of Bioactive Glass and Photocrosslinkable Poly(ϵ -Caprolactone) by Stereolithography. *Compos. Sci. Technol.* **2013**, *74*, 99–106.
- (38) Reid, A. J.; de Luca, A. C.; Faroni, A.; Downes, S.; Sun, M.; Terenghi, G.; Kingham, P. J. Long Term Peripheral Nerve Regeneration Using a Novel PCL Nerve Conduit. *Neurosci. Lett.* **2013**, *544*, 125–130.
- (39) Chung, T.-W.; Yang, M.-C.; Tseng, C.-C.; Sheu, S.-H.; Wang, S.-S.; Huang, Y.-Y.; Chen, S.-D. Promoting Regeneration of Peripheral Nerves in-Vivo Using New PCL-NGF/Tirofiban Nerve Conduits. *Biomaterials* **2011**, *32* (3), 734–743.
- (40) van Bochove, B.; Hannink, G.; Buma, P.; Grijpma, D. W. Preparation of Designed Poly(trimethylene Carbonate) Meniscus Implants by Stereolithography: Challenges in Stereolithography. *Macromol. Biosci.* **2016**, *16* (12), 1853–1863.
- (41) Schüller-Ravoo, S.; Feijen, J.; Grijpma, D. W. Preparation of Flexible and Elastic Poly(trimethylene Carbonate) Structures by Stereolithography. *Macromol. Biosci.* **2011**, *11* (12), 1662–1671.
- (42) Geven, M. A.; Varjas, V.; Kamer, L.; Wang, X.; Peng, J.; Eglin, D.; Grijpma, D. W. Fabrication of Patient Specific Composite Orbital Floor Implants by Stereolithography. *Polym. Adv. Technol.* **2015**, *26* (12), 1433–1438.
- (43) Arcaute, K.; Mann, B. K.; Wicker, R. B. Fabrication of Off-the-Shelf Multilumen Poly(Ethylene Glycol) Nerve Guidance Conduits Using Stereolithography. *Tissue Eng. Part C Methods* **2011**, *17* (1), 27–38.

- (44) Dinis, T. M.; Elia, R.; Vidal, G.; Dermigny, Q.; Denoeud, C.; Kaplan, D. L.; Egles, C.; Marin, F. 3D Multi-Channel Bi-Functionalized Silk Electrospun Conduits for Peripheral Nerve Regeneration. *J. Mech. Behav. Biomed. Mater.* **2015**, *41*, 43–55.
- (45) Bozkurt, A.; Deumens, R.; Beckmann, C.; Olde Damink, L.; Schügner, F.; Heschel, I.; Sellhaus, B.; Weis, J.; Jahnen-Dechent, W.; Brook, G. A.; Pallua, N. In Vitro Cell Alignment Obtained with a Schwann Cell Enriched Microstructured Nerve Guide with Longitudinal Guidance Channels. *Biomaterials* **2009**, *30* (2), 169–179.
- (46) Muheremu, A.; Ao, Q. Past, Present, and Future of Nerve Conduits in the Treatment of Peripheral Nerve Injury. *Biomed Res. Int.* **2015**, *2015*.
- (47) Rivers, T. J.; Hudson, T. W.; Schmidt, C. E. Synthesis of a Novel, Biodegradable Electrically Conducting Polymer for Biomedical Applications. *Adv. Funct. Mater.* **2002**, *12* (1), 33.
- (48) Zhou, C.; Liu, B.; Huang, Y.; Zeng, X.; You, H.; Li, J.; Zhang, Y. The Effect of Four Types of Artificial Nerve Graft Structures on the Repair of 10-Mm Rat Sciatic Nerve Gap. *J. Biomed. Mater. Res. Part A* **2017**, *105* (11), 3077–3085.
- (49) Rodríguez-Vázquez, M.; Vega-Ruiz, B.; Ramos-Zúñiga, R.; Saldaña-Koppel, D. A.; Quiñones-Olvera, L. F. Chitosan and Its Potential Use as a Scaffold for Tissue Engineering in Regenerative Medicine. *Biomed Res. Int.* **2015**, *2015*, 821279.
- (50) Wang, Y.; Zhao, Y.; Sun, C.; Hu, W.; Zhao, J.; Li, G.; Zhang, L.; Liu, M.; Liu, Y.; Ding, F.; Yang, Y.; Gu, X. Chitosan Degradation Products Promote Nerve Regeneration by Stimulating Schwann Cell Proliferation via miR-27a/FOXO1 Axis. *Mol. Neurobiol.* **2016**, *53* (1), 28–39.
- (51) Gloster, A.; Wu, W.; Speelman, A.; Weiss, S.; Causing, C.; Pozniak, C.; Reynolds, B.;

- Chang, E.; Toma, J. G.; Miller, F. D. The T Alpha 1 Alpha-Tubulin Promoter Specifies Gene Expression as a Function of Neuronal Growth and Regeneration in Transgenic Mice. *J. Neurosci.* **1994**, *14* (12), 7319–7330.
- (52) Sun, B.; Zhou, Z.; Wu, T.; Chen, W.; Li, D.; Zheng, H.; El-Hamshary, H.; Al-Deyab, S. S.; Mo, X.; Yu, Y. Development of Nanofiber Sponges-Containing Nerve Guidance Conduit for Peripheral Nerve Regeneration in Vivo. *ACS Appl. Mater. Interfaces* **2017**, *9* (32), 26684–26696.
- (53) Glenn, T. D.; Talbot, W. S. Signals Regulating Myelination in Peripheral Nerves and the Schwann Cell Response to Injury. *Curr. Opin. Neurobiol.* **2013**, *23* (6), 1041–1048.
- (54) Bozkurt, A.; Boecker, A.; Tank, J.; Altinova, H.; Deumens, R.; Dabhi, C.; Tolba, R.; Weis, J.; Brook, G. A.; Pallua, N.; van Neerven, S. G. A. Efficient Bridging of 20 Mm Rat Sciatic Nerve Lesions with a Longitudinally Micro-Structured Collagen Scaffold. *Biomaterials* **2016**, *75*, 112–122.
- (55) Rich, K. M.; Alexander, T. D.; Pryor, J. C.; Hollowell, J. P. Nerve Growth Factor Enhances Regeneration through Silicone Chambers. *Exp. Neurol.* **1989**, *105* (2), 162–170.

Figures:

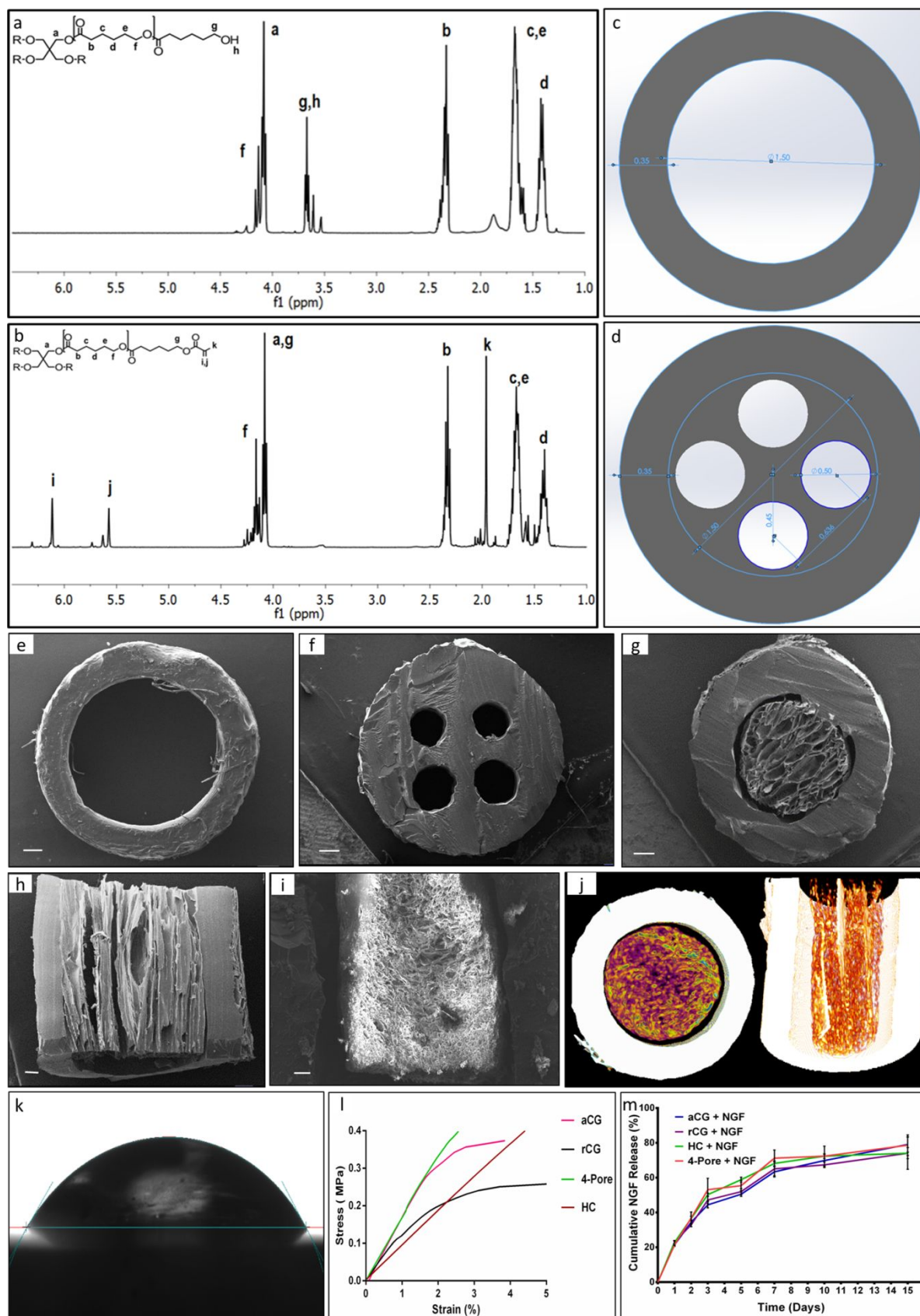


Figure 1. Fabrication and characterization of 3D printed PCL NGCs. **a,b**, ¹H NMR spectrum of PCL oligomer (**a**) and methacrylated PCL oligomer (**b**). **c,d**, Axial view of designs for hollow (**c**) and 4-Pore (**d**) NGCs. Fabrication and characterization of 3D printed-cryogel based nerve guidance channels. **e-i**, Representative SEM micrographs of transverse sections of hollow (**e**), 4-pore (**f**), aCG, Scale bar 200 μm (**g**), longitudinal section of aCG, Scale bar 100 μm (**h**), longitudinal section of rCG, Scale bar 100 μm (**i**), NGCs. **j**, Micro-CT image of transverse and longitudinal section of aCG NGCs. **k**, Surface hydrophilicity of 3D printed PCL sheet by contact angle measurement. **l**, Stress vs strain curve of uniaxial tensile testing of NGCs. **m**, Cumulative NGF release kinetics from NGCs.

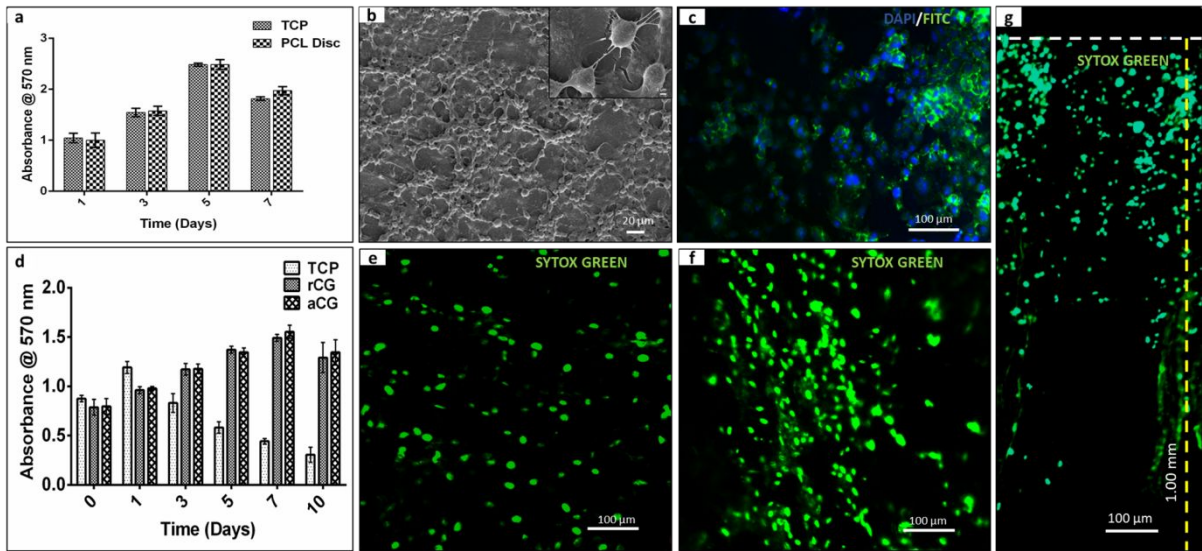


Figure 2. In-vitro cell material interaction studies. **a**, Cell metabolic activity studies on 3D printed PCL discs by MTT assay for 7 days. **b**, Representative SEM micrographs of Neuro2a cells on PCL disc, scale bar 20 μm (**b**) at higher magnification (inset), scale bar 2 μm. **c**, DAPI/FITC fluorescence image of Neuro2a cells on PCL disc at day 5 showing cell material interaction, cell adherence and proliferation, scale bar 100 μm. **d**, Cell metabolic activity on aligned (aCG), random (rCG) NGCs and 2D culture by MTT assay for 10 days. **e-g**, Representative SYTOX Green fluorescence imaging of Neuro2a cells at day 5 on random (rCG) (**e**) aligned (aCG) (**f**) NGCs, (scale bar 100 μm at 20x magnification), enlarged image showing Neuro2a cellular infiltration deep into aligned NGCs (**g**), where, white dashed line represents the top surface of scaffold, (scale bar 100 μm at 10x magnification).

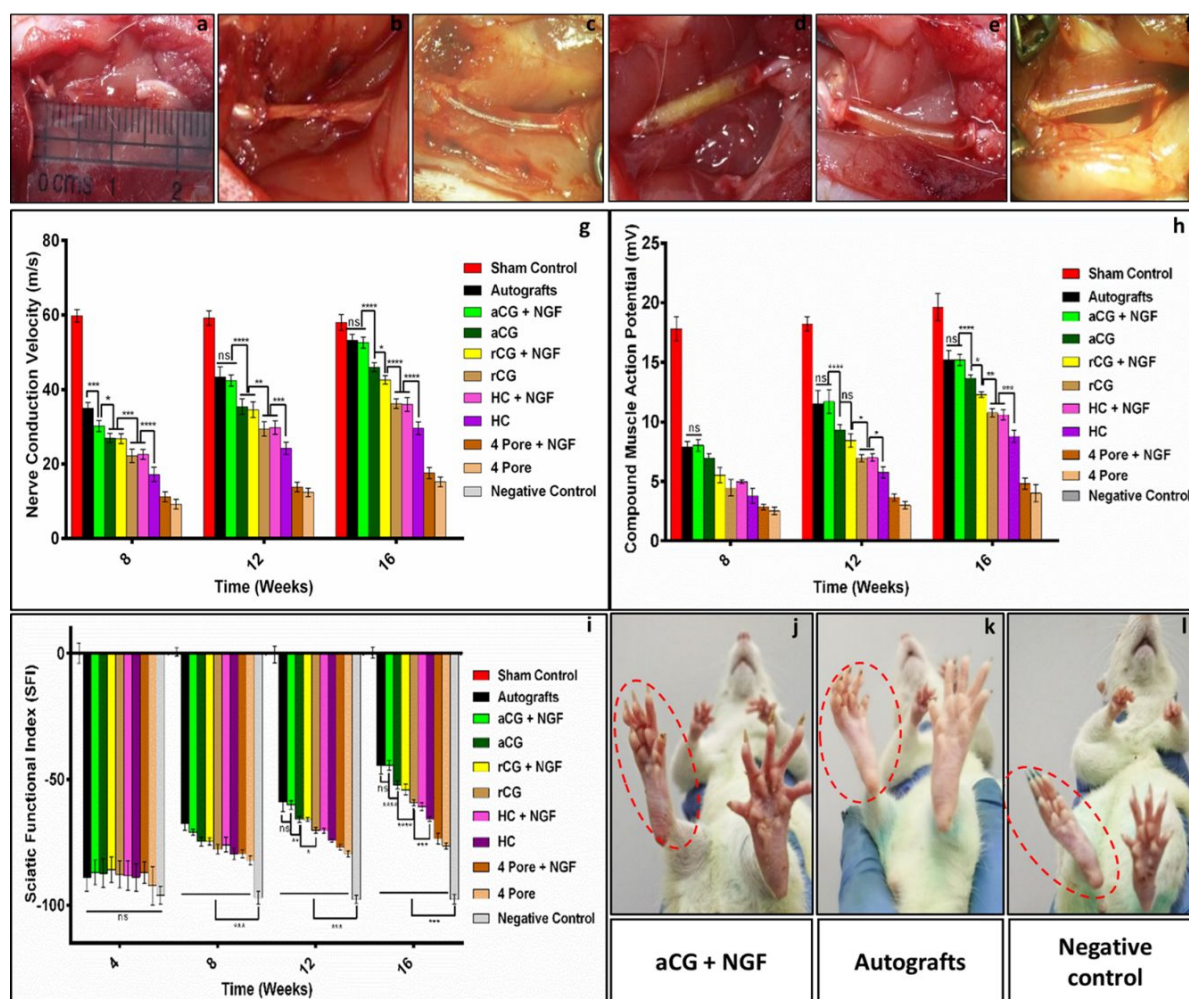


Figure 3. a-f, Photographs of nerve guidance channels immediately after implantation in negative control group (a), autografts (b), HC (c), rCG (d), aCG (e), 4-Pore (f), NGCs. g,h, Quantitative analysis of functional regeneration by measuring electrophysiological parameters such as nerve conduction velocity (NCV) (g) and compound muscle action potential (CMAP) (h) after specified time intervals. i, Quantitative analysis of sciatic nerve functional index (SFI) calculated by walking track analysis at 4, 8, 12 and 16 weeks post-surgery. j-l, Photographs showing improvement in paw spreading after 16 weeks in aCG+NGF (j), autografts (k), and negative control (l) groups.

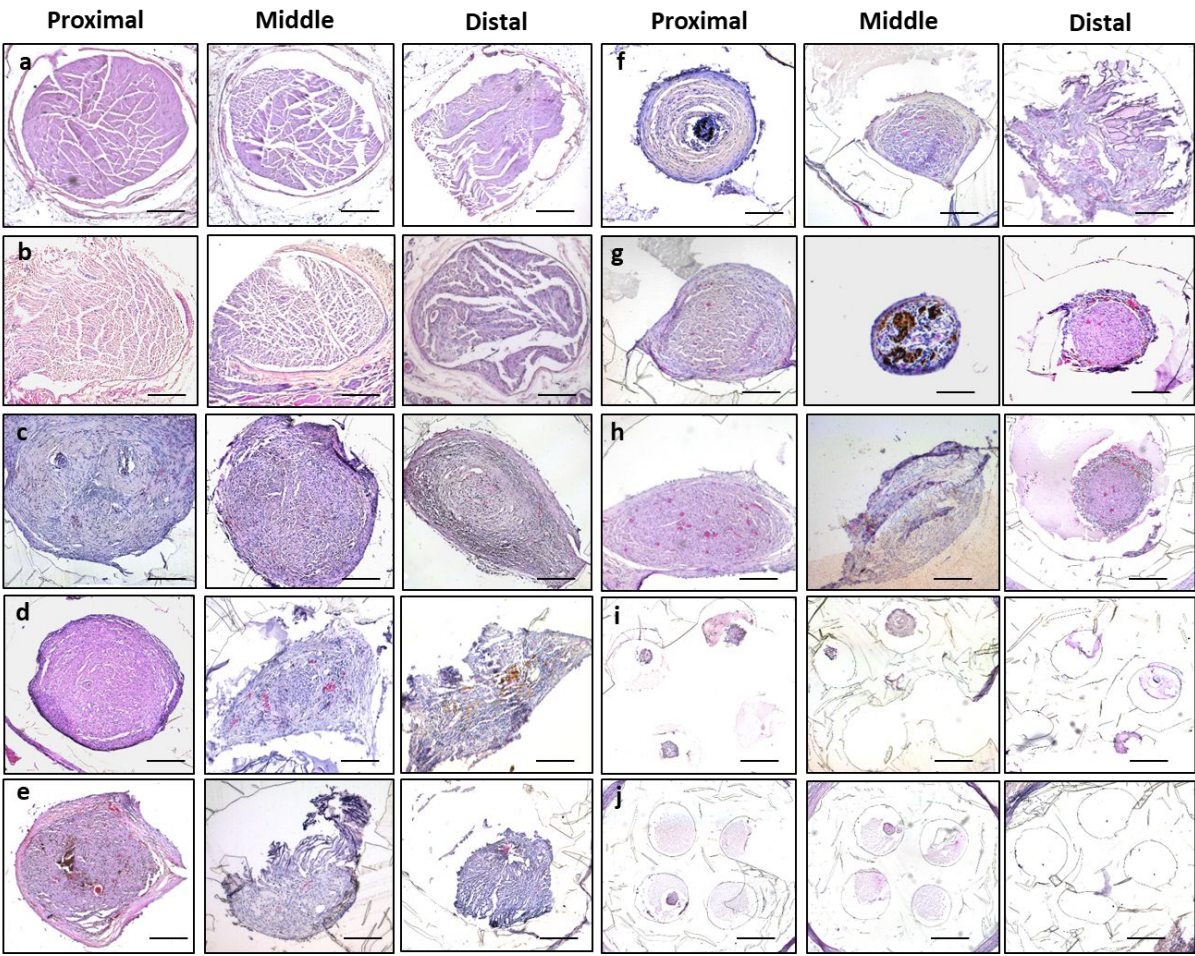


Figure 4. Histological examination of the regenerated nerve tissue by H&E staining **a-j**, Proximal, middle and distal portions of the harvested nerve after 16 weeks' post-surgery of sham control (**a**), autografts (**b**), aCG+NGF (**c**), aCG (**d**), rCG+NGF (**e**), rCG (**f**), HC+NGF (**g**), HC (**h**), 4P+NGF (**i**) and 4P (**j**) NGCs. Scale bar = 200 μ m.

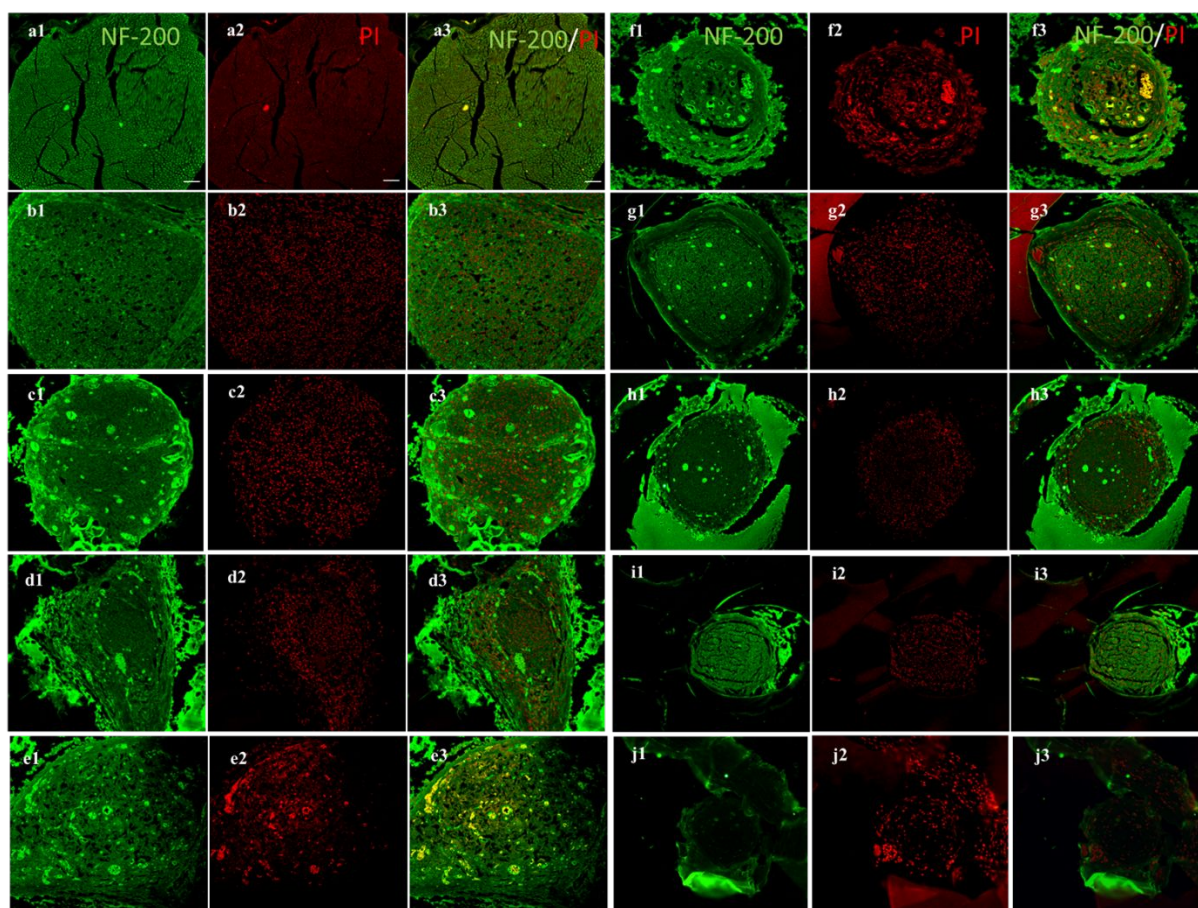


Figure 5. Immunofluorescence examination of the regenerated nerve tissue for neurofilament NF-200 (green)/PI (red) staining. **a-j**, Middle portions of the harvested nerve after 16 weeks' post-surgery of sham control (**a**), autografts (**b**), aCG+NGF (**c**), aCG (**d**), rCG+NGF (**e**), rCG (**f**), HC+NGF (**g**), HC (**h**), 4P+NGF (**i**) and 4P (**j**) NGCs. Scale bar = 50 μ m.

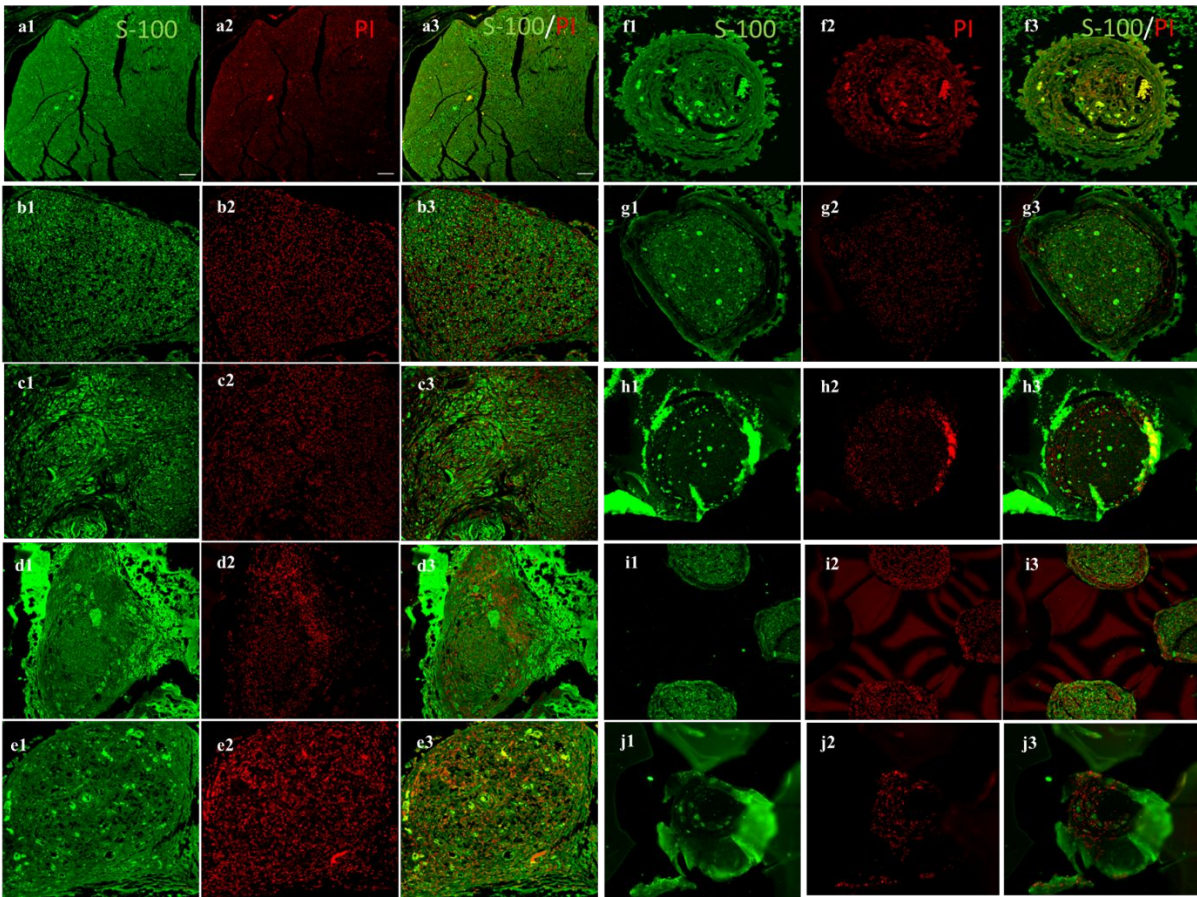


Figure 6. Immunofluorescence examination of the regenerated nerve tissue for Schwann cell marker S-100 (green)/PI (red) staining. **a-j**, Middle portions of the harvested nerve after 16 weeks post-surgery of sham control (**a**), autografts (**b**), aCG+NGF (**c**), aCG (**d**), rCG+NGF (**e**), rCG (**f**), HC+NGF (**g**), HC (**h**), 4P+NGF (**i**) and 4P (**j**) NGCs. Scale bar = 50 μm.

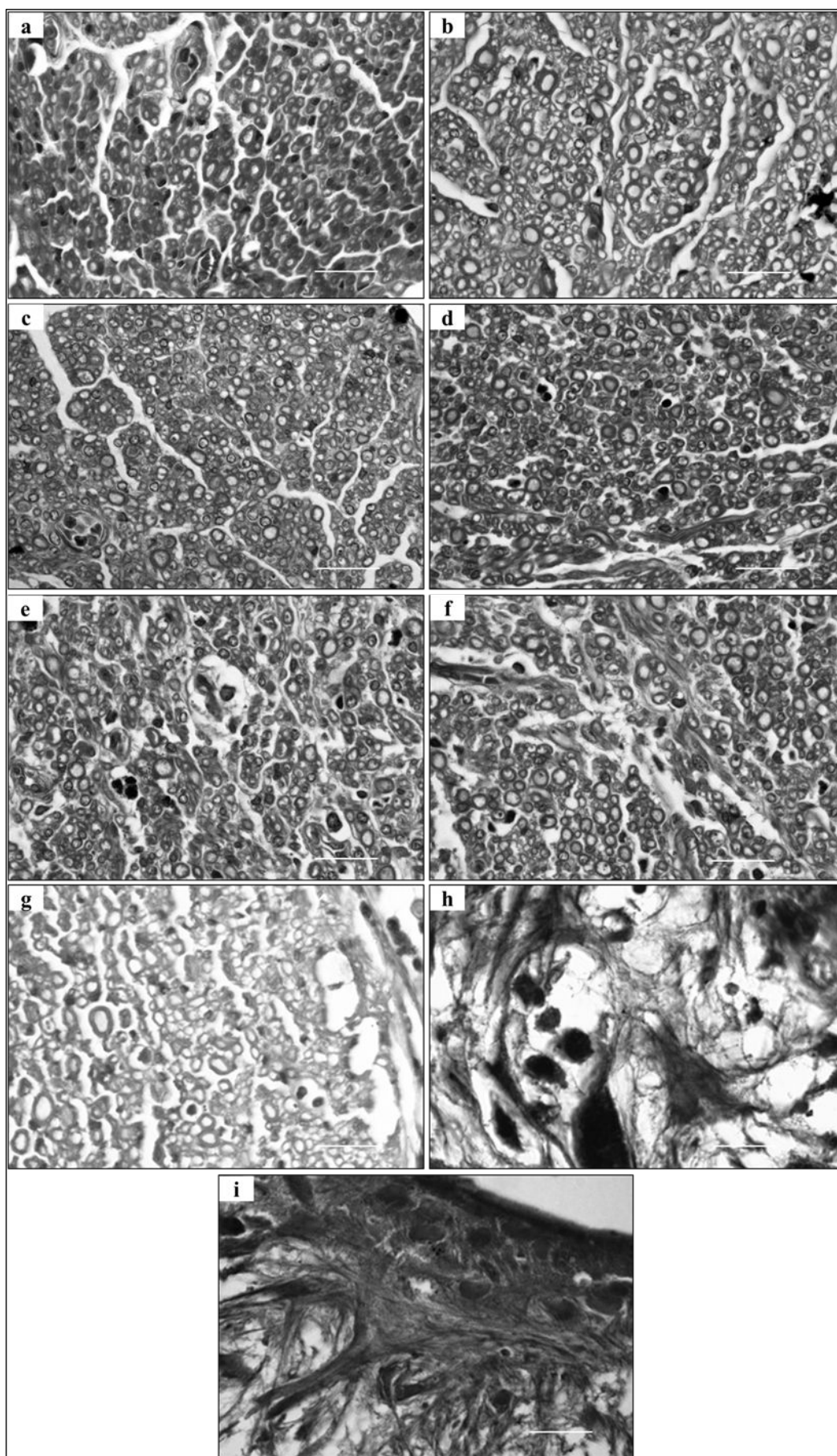


Figure 7. a-i, Light micrographs of toluidine blue stained transverse sections of middle segment from regenerated nerve of autografts **(a)**, aCG+NGF **(b)**, aCG **(c)**, rCG+NGF **(d)**, rCG **(e)**, HC+NGF **(f)**, HC **(g)**, 4P+NGF **(h)**, 4P **(i)** NGCs. Scale bar 20 μm . The images are represented in grayscale for better visualization.

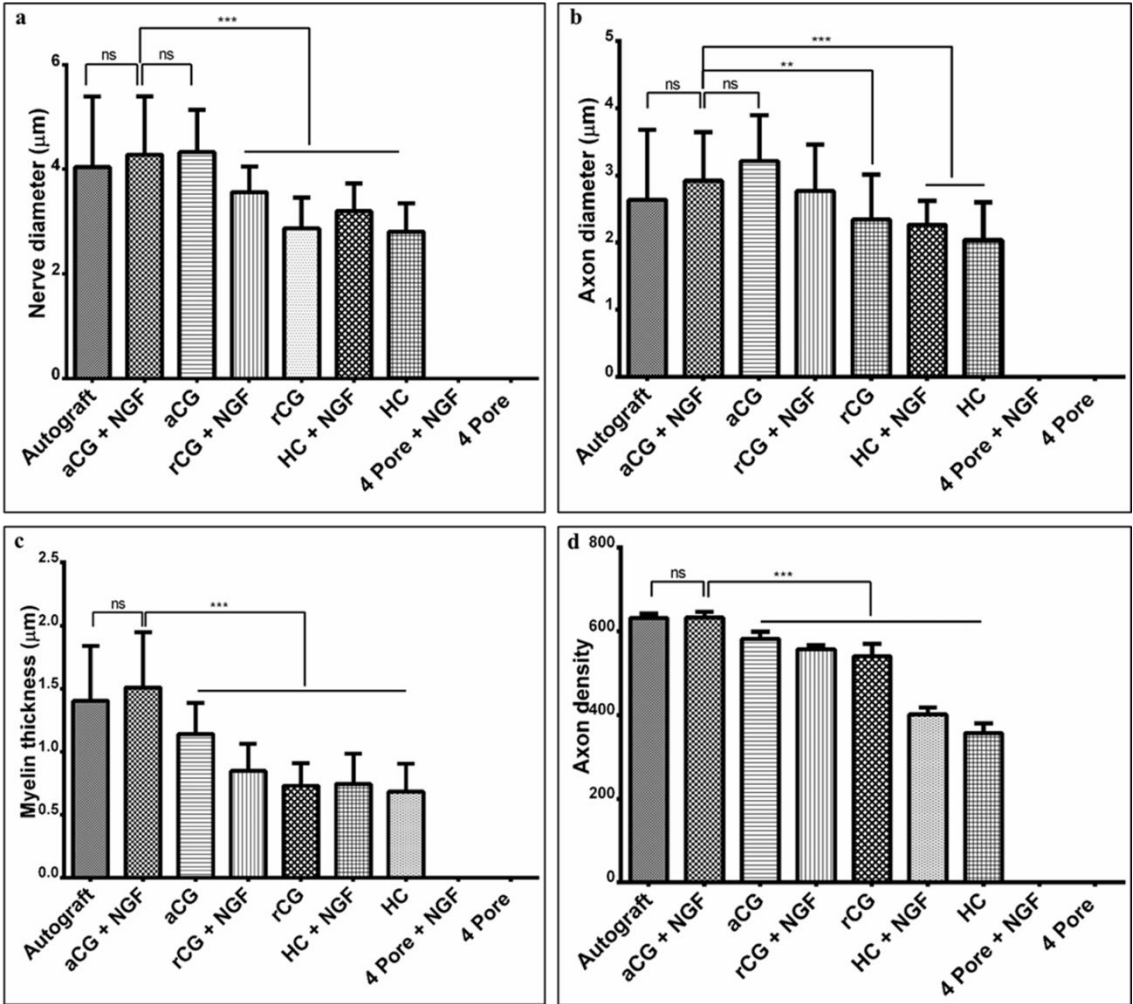


Figure 8. a-d, Morphometric analysis for axonal regeneration from middle transverse sections after 16 weeks' of implantation of nerve diameter **(a)**, axon diameter **(b)**, myelin thickness **(c)** and axon density **(d)**. * $p \leq 0.05$, ** $p \leq 0.01$, *** $p \leq 0.001$, ns: non-significant.

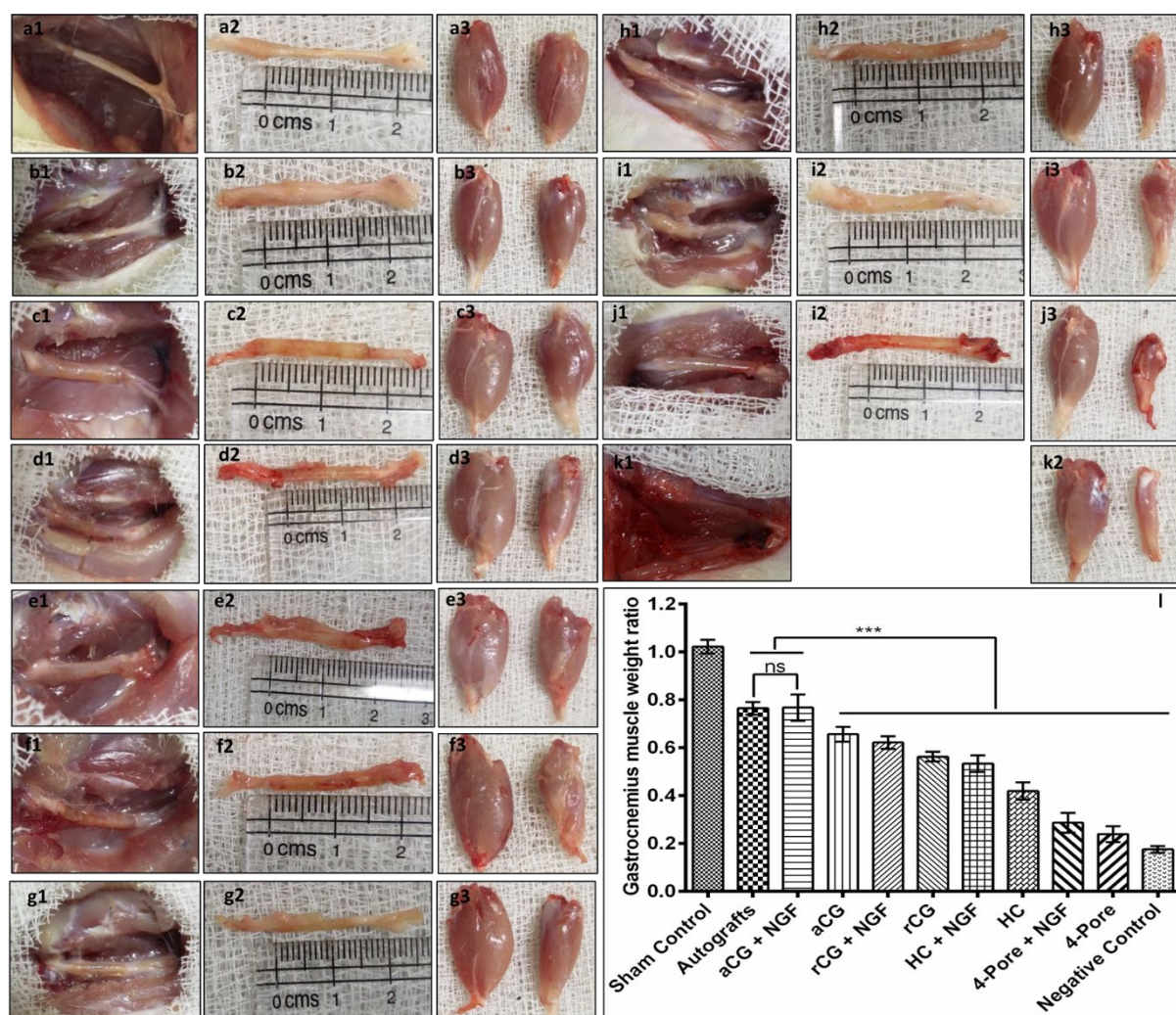


Figure 9. a-k, Photographs showing regenerated sciatic nerve (left), harvested nerve tissue (middle) and gastrocnemius muscle (right) in all different experimental groups after 16 weeks' post implantation of sham control (a), autografts (b), aCG+NGF (c), aCG (d), rCG+NGF (e), rCG (f), HC+NGF (g), HC (h), 4P+NGF (i), 4P (j), and negative control (k) groups. **l,** Histograms comparing the gastrocnemius muscle weight ratio harvested from different experimental groups. *** $p \leq 0.001$, ns: non-significant.

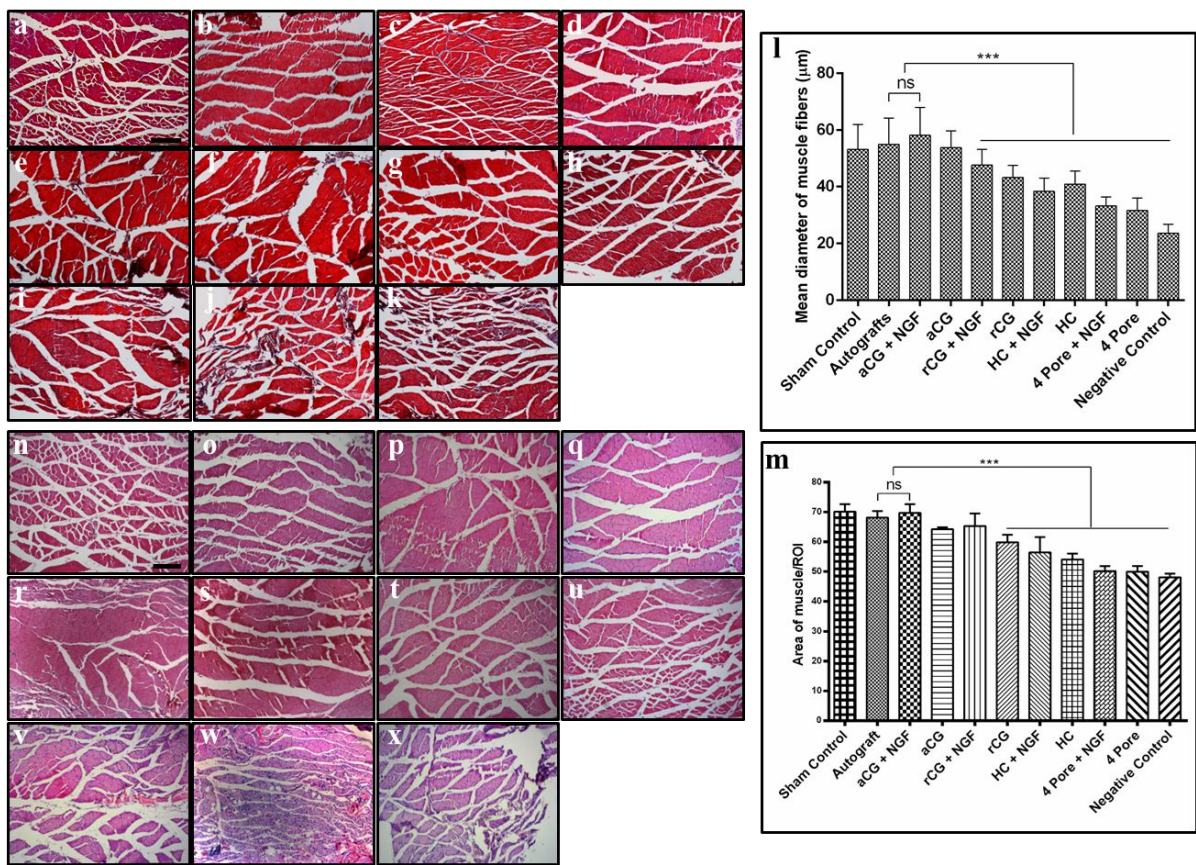


Figure 10. Gastrocnemius muscle analysis. **a-k**, Masson's trichrome staining of sham control (**a**), autografts (**b**), aCG+NGF (**c**), aCG (**d**), rCG+NGF (**e**), rCG (**f**), HC+NGF (**g**), HC (**h**), 4P+NGF (**i**), 4P (**j**), and negative control (**k**) groups. Scale bar = 200 μm. **l,m**, Histomorphometric analysis of transverse sections for measurement of mean diameter of muscle fiber (**l**) and area of muscle per region of interest (ROI) (**m**). **n-x**, H&E staining images of sham control (**n**), autografts (**o**), aCG+NGF (**p**), aCG (**q**), rCG+NGF (**r**), rCG (**s**), HC+NGF (**t**), HC (**u**), 4P+NGF (**v**), 4P (**w**), and negative control (**x**) groups. Scale bar = 200 μm. *** $p \leq 0.001$, ns: non-significant.

Table 1: Experimental groups used in the study

Animal Groups	No. of animals	Description of implanted NGCs
aCG+NGF	6	Aligned chitosan-gelatin cryogel filled NGC with NGF
aCG	6	Aligned chitosan-gelatin cryogel filled NGC
rCG+NGF	6	Random chitosan-gelatin cryogel filled NGC with NGF
rCG	6	Random chitosan-gelatin cryogel filled NGC
HC+NGF	6	Hollow conduit with NGF
HC	6	Hollow conduit
4P+NGF	6	4-Pore multichannel conduit with NGF
4P	6	4-Pore multichannel conduit
Negative Control	6	No treatment
Autografts	6	Nerve sutured in reversed direction
Sham Control	5	Surgical intervention without nerve injury

Table 2: NCV and CMAP of experimental groups after 16 weeks post implantation

Experimental Groups	NCV (m/s)	CMAP (mV)
aCG+NGF	52.60 ± 1.51	15.20 ± 0.45
aCG	46.00 ± 1.22	13.66 ± 0.27
rCG+NGF	42.60 ± 1.14	12.28 ± 0.25
rCG	36.20 ± 1.30	10.76 ± 0.33
HC+NGF	36.00 ± 1.87	10.60 ± 0.42
HC	29.60 ± 1.67	8.78 ± 0.52
4-Pore+NGF	17.6 ± 1.51	4.80 ± 0.46
4-Pore	15.20 ± 1.30	4.00 ± 0.73
Negative Control	0.0 ± 0.0	0.0 ± 0.0
Autografts	53.2 ± 1.64	15.22 ± 0.80
Sham Control	58.00 ± 2.12	19.62 ± 1.13

Table of contents: